Table of Contents

1. A Hybrid Microcalcification Detection Algorithm In Digital Mammograms
Page 1-7
--*Ping Zhang, Kwabena Agyepong*

2. An Improved Iterative Watershed According to Ridge Detection for Segmentation of Metallographic Image
Page 8-13
--*Jiangbo Liu, Jianxun Chen*

3. The Use of Geospatial Information Systems in the Analysis of Pollution Trends in Southern Mississippi Region
Page 14-29
--*Edmund C.Merem, Yaw.A.Twumasi, Sudha.Yerramilli, Chandra Richardson*

4. A Joint Scheduling and Mapping Method for Dynamically Reconfigurable SoCs Interconnected by an on-chip Mesh Network
Page 30-39
--*Ling Wang, Xiangnan Sui, Yingtao Jiang*

A Hybrid Microcalcification Detection Algorithm In Digital Mammograms

Ping Zhang[a], Kwabena Agyepong[b]

[a] Department of Mathematics and Computer Science
[b] Department of Advanced Technologies
Alcorn State University, Mississippi 39096-7500, USA

Abstract—A novel hybrid wavelet-based fractal feature extraction method is proposed for the detection of microcalcification clusters (MCCs) in digital mammograms. The hybrid features consists of a set of the surrounding region dependence based features [11] and the newly proposed wavelet-based fractal features. A new fractal feature extraction scheme is given in this paper, which is based on the wavelet coefficients of a mammography image. Experiments demonstrated that the proposed hybrid features have the best convergence ability of artificial neural networks (ANNs) classifier compared to other two sets of features tested in the experiments. A good ratio of true positive fraction to false positive fraction (ROC curve) has been achieved. The proposed MCCs detection system provides an adequate framework for microcalcification detection in mammograms.

Keywords—pattern recognition, hybrid feature extraction, ANN classifier, calcification detection

I. Introduction

Breast cancer can be divided into three categories: microcalcifications, masses, and architectural distortions. An early sign of breast cancer is the presence of microcalcification clusters (MCCs) in the mammogram. MCCs are small in size and have low contrast that may be missed or misinterpreted by physicians and the task of eye-based mammography screening is tedious; therefore, a reliable and automatic computer-aided diagnosis system (CADx) could be very helpful to aid radiologists in detecting mammography lesions that may indicate the presence of breast cancer.

Microcalcifications are tiny deposits of calcium which appear as small bright spots on the mammogram. Microcalcifications are characterized by clusters, types, and distribution properties. Fig.1 shows two images of MCCs (a, b) and two images of normal mammogram (c, d).

Microclacification image analysis and detection is an extremely challenging task for the following three reasons: First of all, there is a large variability in the appearance of abnormalities. Likewise, abnormalities are often occluded or hidden in dense breast tissue. Perhaps most importantly, a CADx system for MCCs detection is used in serious human disease detection; hence, a need for near faultlessness is required.

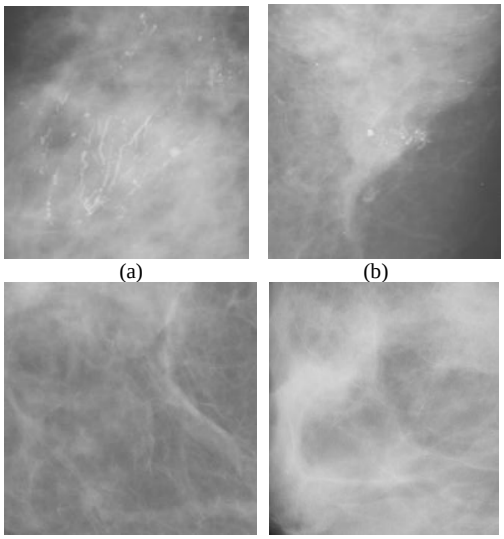

Fig. 1. Four mammograms: (a, b) calcification images; (c, d) normal images

Concerning calcification detection in the regions of interests (ROIs), many methods have been proposed. In the survey paper [1], mammogram enhancement and segmentation algorithms, mammographic features, classifiers and their performances were reviewed and compared. Remaining challenges were also discussed. In another paper [2], the detection performances of different classifiers, such as Support Vector Machines (SVMs), Kernel Fisher discriminant (KFD) classifier, Relevance Vector Machine (RVM), and committee machines (ensemble averaging and AdaBoost) were compared and the test results were reported. Neural networks have been used in many calcification systems. Two automatic microcalcification detection

Corresponding Author: Ping Zhang, Email Address: pzhang@alcorn.edu

systems were proposed based on the hybrid neural network classifier [3, 4]. SVMs have been used in the mammogram detection systems [5, 6]. Unsupervised detection of mammogram ROIs was introduced [7]. Segmentation of ROIs in mammogram using a topographic approach was introduced in the recent literature [8].

Feature extraction is one of the most important components in mammogram detection. A local feature extraction has been adopted in the literature more than a decade ago [9]. For example, the application of shape analysis to mammographic calcification was introduced [10]. A statistical textural feature for the detection of microcalcification was described in the reference [11]. Wavelets have been widely used in the feature extraction and segmentation in the mammogram detection [12-16]. Combining mathematical morphology and neural networks was also proposed in the literature [17] and multifractal analysis has been used in the medical image detection and classification [18-20].

In order to increase detection rate, a multiple expert system was given in the detection system [21]. A fuzzy logic was then introduced to detect calcification [22]. A microcalcifications detection algorithm by fitting a model to every location in the mammogram was proposed [23].

Artificial Neural Networks (ANNs) have been considered as efficient classifiers in many pattern recognition systems. Typically, an ANN accepts inputting features, which are computed from a specific region of interest, and provides an output as a characterization of the region [11].

In this paper, a microcalcification detection system with a novel hybrid feature extraction scheme is proposed. A system flowchart is drawn in Section II. Hybrid feature extraction method is presented in Section III, which concatenates the following feature sets: Surrounding Region Dependence Based (SRDM) feature set + Wavelet-based multifractal feature set. The specification of an ANN classifier is listed in Section IV. The experimental comparisons on calcification detection performance have been conducted on three ANN classifiers, which were trained by three sets of features. The testing results are reported in Section V. The conclusion is given in the last section.

II. Digital Mammogram Detection System

The schematic diagram of the proposed system is shown in Fig. 2. The system includes five components: ROI image input, image preprocessing, hybrid feature extraction, ANN classifier design and detection output.

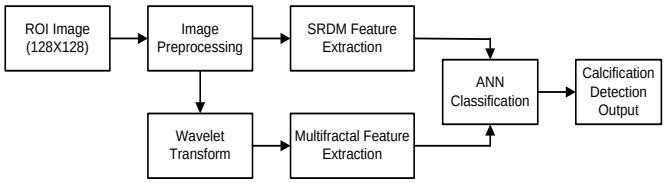

Fig. 2. Schematic diagram for microcalcification cluster detection

Image preprocessing includes the following operations on mammograms: image contrast enhancement, noise removal and histogram equalization in order to retain small spots (calcification feature) in the mammograms. For the detail image preprocessing algorithms, the interested readers can refer to image processing book [30].

Hybrid feature extraction method is divided into three steps: SRDM feature extraction, wavelet transform, and wavelet-based multifractal feature extraction.

III. Hybrid Feature Extraction

Feature extraction and classifier design are two of the most important steps in the design of a pattern recognition system. We will discuss three sets of features as follows:

3.1. Surrounding Region Dependence Based Method (SRDM)

A simple surrounding region dependence based method [11] is used as a first feature set. Firstly, the microcalfication area of a mammogram is divided into different overlapping 128x128 blocks (The image block size of 128x128 is considered based on mammogram resolution and computation simplicity); then the first feature set is extracted from each block. In order to systematically address this feature set, the diagram of the surrounding regions for current pixel *(x, y)* is shown in Fig. 3. Here, $\boldsymbol{R_1}$ and $\boldsymbol{R_2}$ are the inner surrounding region and the outer surrounding region, respectively. w_1, w_2, and w_3 denote the size of the three square windows.

In the following calculations, *n* is the maximal pixel number of R1 (inner region); *m* is the maximal pixel number of R2 (outer region).

$$\alpha(i,j) = \#\{(x,y) \mid c_{R_1}(x,y) = i, c_{R_2}(x,y) = j, (x,y) \in L_x \times L_y\}$$
$$c_{R_1}(x,y) = \#\{(k,l) \mid (k,l) \in R_1, [S(x,y) - S(k,l)] > q\}$$

$$c_{R_2}(x,y) = \#\{(k,l) \mid (k,l) \in R_2, [S(x,y) - S(k,l)] > q\}$$

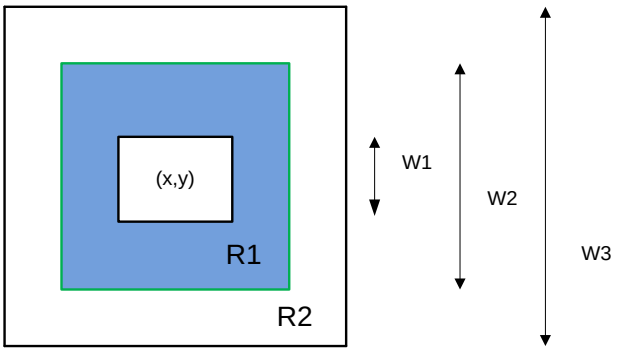

Fig. 3. Diagram of the surrounding regions

where *S(x, y)* is the image intensity of the current pixel (x, y), parameter *q* is a constant. # equates the number of pixels. *r(i,j)* is the reciprocal of the element, which is calculated as follows:

$$r(i,j) = \begin{cases} \dfrac{1}{\alpha(i,j)} & \text{if } \alpha(i,j) > 0 \\ 0 & \text{otherwise} \end{cases} \quad (1)$$

The following features are extracted:

Horizontal-weighted sum (HWS)

$$HWS = \frac{1}{N}\sum_{i=0}^{m}\sum_{j=0}^{n} j^2 r(i,j) \quad (2)$$

Vertical-weighted sum (VWS)

$$VWS = \frac{1}{N}\sum_{i=0}^{m}\sum_{j=0}^{n} i^2 r(i,j) \quad (3)$$

Diagonal-weighted sum (DWS)

$$DWS = \frac{1}{N}\sum_{k=0}^{m+n} k^2 \sum_{\substack{i=0 \\ i+j=k}}^{m}\sum_{j=0}^{n} r(i,j) \quad (4)$$

Grid-weighted sum (GWS)

$$GWS = \frac{1}{N}\sum_{i=0}^{m}\sum_{j=0}^{n} ijr(i,j) \quad (5)$$

where N is the total sum of elements in the surrounding region, which is defined as below:

$$N = \sum_{i=0}^{m}\sum_{j=0}^{n} \alpha(i,j) \quad (6)$$

Except for above mentioned four features, additional four new features are added in our system [24].

Variance sum (VS)

$$VS = \sum_{i=0}^{N_x-1}\sum_{j=0}^{N_y-1} (S(i,j) - \overline{S})^2 \quad (7)$$

Discrete Laplacian sum (DLS)

$$DLS = \sum_{i=0}^{N_x-1}\sum_{j=0}^{N_y-1} \frac{1}{4}\left(\frac{\partial^2 S(i,j)}{\partial i^2} + \frac{\partial^2 S(i,j)}{\partial j^2}\right) \quad (8)$$

Entropy (E)

$$E = -\sum_{i=0}^{N_x-1}\sum_{j=0}^{N_y-1} P(i,j)\log_2 P(i,j) \quad (9)$$

Mean Grey Level (MGL)

$$MGL = \frac{1}{N_x * N_y}\sum_{i=0}^{N_x-1}\sum_{j=0}^{N_y-1} S(i,j) \quad (10)$$

where N_x, N_y is the size of selected mammogram. In total, eight (8) features are extracted as texture features.

3.2. Wavelet Transform

The definition of a continuous wavelet transform is as follows[25]: for a continuous function *f(x)*, it is projected at each step *j* on the subset V_j, *(……⊂ V_{-1}⊂ V_0⊂ V_1⊂ V_2⊂...)*. The scalar project $c_{j,k}$ is defined by the dot product of *f(x)* with the scaling function $\phi(x)$, which is dilated and translated:

$$c_{j,k} = < f(x), \phi_{j,k}(x) >$$
$$\phi_{j,k}(x) = 2^{j/2}\phi(2^j x - k) \quad (11)$$

The difference between $c_{j+1,k}$ and $c_{j,k}$ is contained in the detailed component belonging to the space W_j, which is orthogonal to V_j. The following equations exist:

$$W_j \oplus V_j = V_{j+1}$$
$$V_j \cap W_j = \{0\},\ j \in Z \quad (12)$$

Suppose $\psi(x)$ is a wavelet function. The wavelet coefficients can be obtained by

$$w_{j,k} = < f(x), 2^{j/2}\psi(2^j x - k) > \quad (13)$$

Some relationships between $\phi(x)$ and $\psi(x)$ are listed below:

$$\tfrac{1}{2}\phi(\tfrac{x}{2}) = \sum_n h(n)\phi(x-n)$$
$$\tfrac{1}{2}\psi(\tfrac{x}{2}) = \sum_n g(n)\phi(x-n) \quad (14)$$

where *h(n)* and *g(n)* represent unit impulse functions of lowpass and highpass filters respectively, which are related to the scaling function $\phi(x)$ and the wavelet function $\psi(x)$.

According to the wavelet theory, a conventional two dimensional wavelet discrete transform (2D-DWT) can be regarded as being equivalent to filtering the input image with a bank of filters, whose impulse responses are all approximately given by scaled versions of a mother wavelet. The output of each level consists of four sub-images: *LL, LH, HL, HH* with 2:1 down-sampling.

Mathematically, we can express this recursive algorithm in the following equation.

$$\begin{aligned}\psi(x,y)_{LL} &= \phi(x)\phi(y)\\ \psi(x,y)_{LH} &= \phi(x)\psi(y)\\ \psi(x,y)_{HL} &= \psi(x)\phi(y)\\ \psi(x,y)_{HH} &= \psi(x)\psi(y)\end{aligned} \tag{15}$$

For example, The *LL* wavelet is the product of the low-pass function $\phi(x)$ along both the first dimension and second dimension; The *LH* wavelet is the product of the low-pass function $\phi(x)$ along the first dimension and the high-pass function $\psi(y)$ along the second dimension.

If the wavelet filters are real, then Mallat's dyadic wavelet decomposition fast algorithm [25] can be used. However, 2D-DWT has the following drawbacks: lack of shift invariance and poor directional selectivity.

3.3. Wavelet-based Multifractal Feature

The fractal application to image classification and recognition is receiving a lot of attention. The term fractal was coined by Mandelbrot in 1975 to describe the irregular structure of many natural objects and phenomena. Central to fractal geometry is the concept of self-similarity. Considering a bounded set ***R*** in Euclidean *n*-space, the set is said to be self-similar when ***R*** is the union of ***Nr*** distinct (non-overlapping) copies of itself, each of which has been scaled down by a ratio r<1 in all coordinates. The similarity dimension *Ds* is given by

$$N_r \cdot r^{Ds} = 1, \qquad where \qquad Ds = \log(N_r)/\log(1/r) \tag{16}$$

The ranges in the value of *Ds* characterize the type of fractal. A few methods to compute the fractal dimension have been published, such as Walking-Divider, Box Counting, Prism Counting, Epsilon-Blanket, Perimeter-Area Relationship, Fractional Brownian Motion, Power Spectrum, and Hybrid Methods [26]. For example, a simple wavelet-based fractal feature extraction algorithm has been used to recognize similar objects with very high accuracy [27].

Based on successful applications in medical image processing and recognition [28, 29], we proposed a novel feature extraction scheme: Firstly, the ROI of the calcification image is decomposed using 2D-wavelet transformation to create four decomposition subimages: $\boldsymbol{C_{LL}}$, $\boldsymbol{D_{LH}}$, $\boldsymbol{D_{HL}}$ and $\boldsymbol{D_{HH}}$. Then, the coefficients *I(x, y)* of each of the four wavelet subimages are used to calculate fractal number as follows:

$$d(k) = \sum_{x=0}^{M-1}\sum_{y=0}^{N-k-1} |I(x,y) - I(x,y+k)| / (M*(N-k)| + \sum_{y=0}^{N-1}\sum_{x=0}^{M-k-1} |I(x,y) - I(x+k,y)| / (N*(M-k) \tag{17}$$

and

$$F(k) = \log(d(k+1)) - \log(d(1)) \tag{18}$$

where, *k*=1,2,… *l*; *l* is number of feature. A vector of [*F (1), F (2), . ., F (l)*] will be fed into ANN classifier for training and testing.

IV. Classification

A three-layer ANN is used as a classifier. The layout of the ANN classifier is listed as follows:

No. of Input Layer: No. of features

No. of Hidden Layer: 50~100, depending on number of training samples

No. of Output Layer: 2 (Cancer and Normal Case)

Backpropagation algorithm is used in the ANN training procedure.

V. Experiment Results

In order to test the system's flexibility and MCCs detection performance, we conducted two experiments: one is to test classifier's convergence performance on the training set and to evaluate MCCs detection performance on the testing samples by inputting

different feature sets. Another experiment is to estimate MCCs' ROC curve on the testing samples.

One of databases is miniDDSM Database, which was created based on the original DDSM database [31] by the System Research Institute (SRI) at Alcorn State University, USA. The mammograms in the miniDDSM Database have been down-sampled in size. The image intensity is scaled into 256 grey levels.

A training set of 2,000 subimages with size of 128x128 are extracted from the subimages of microcalcification ROIs and the subimages of non-cancer areas. All of the subimages are manually selected from the mniDDSM database. Another set of 100 subimages of ROIs and 100 subimages of non-calcification areas are selected for the test.

In the first experiment, three sets of features (SRDM feature set, SRDM + Wavelet feature set, and SRDM + Wavelet-based fractal feature set) are used to train three ANN classifiers with the same configuration, respectively.

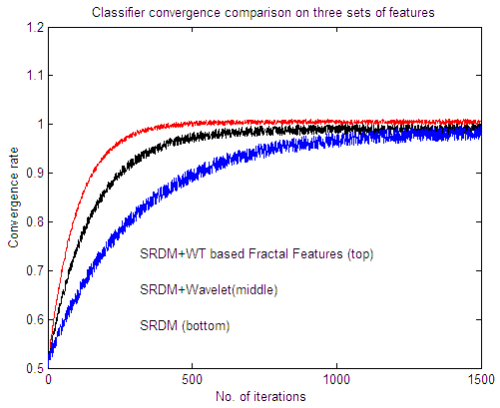

Fig. 4. ANN training convergence comparison on three sets of features

An ANN classifier trained by the third feature set (hybrid feature set: SRDM+ Wavelet-based fractal feature) can achieve the highest detection rate compared to the other two classifiers.

In our experiment, the wavelet feature set is extracted from 4x4 Daubechies wavelet coefficients, which is the result of multilevel 2D wavelet decompositions on ROI (128x128 subimage).

As shown in Fig. 4, the third set of SRDM+Wavelet-based fractal features has the best classifier convergence performance.

In the second experiment, the ROC curves are drawn.

TP (true positive): patient with disease (calcification) is correctly diagnosed.

FN (false negative): patient without disease (calcification) is diagnosed as diseased.

ANN confidence values given by the array: [0.65 0.70 0.75 0.80 0.85] were used for obtaining variation in order to draw the FROC curve. All of the experiments were conducted on a PC computer with a CPU processor of 2.5 GHz. The average speed for detecting a mammogram image is 5 seconds, including image preprocessing, feature extraction, and detection.

We tested on two databases: Mini-MIAS and miniDDSM. The FROC curves obtained are shown below:

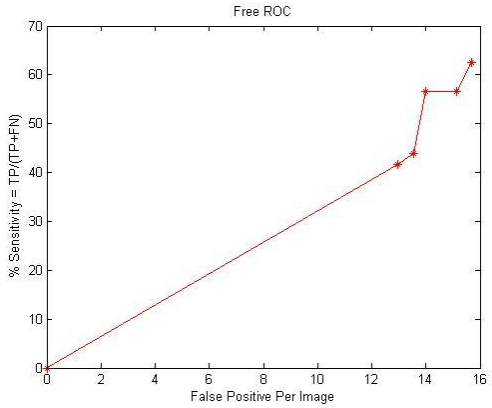

Fig. 5. Calcification detection performance on Mini-MIAS database (using SRDM + Wavelet-based fractal feature set)

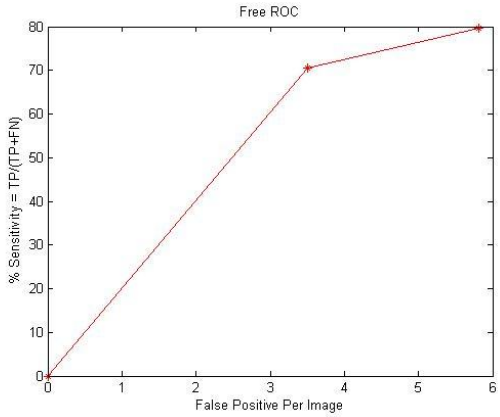

Fig. 6. Calcification detection performance on miniDDSM database (using SRDM + Wavelet-based fractal feature set)

VI. Conclusion

A novel hybrid feature extraction method is proposed and successfully applied to the detection of microcalcifications in digital mammograms. The hybrid feature set consists of the surrounding region dependence based features and wavelet-based fractal features. A merit of the proposed feature extraction method is that wavelet transformation can decompose

a ROI image into different subimages with different frequency bands and direction orientations, which means that the finer feature components may be explored in the 2D-WT. The cascaded fractal feature extraction based on the 2D-WT can overcome some deficiency of the 2D-WT.

The comparative experiments have demonstrated that the proposed feature extraction scheme has the best classifier training convergence performance among three sets of features used in the experiments and the FROC is also reported. Future work will focus on constructing a classification system with ensemble classifiers with hybrid features in order to increase system's reliability and detection rate at the same time in one system.

ACKNOWLEDGEMENTS

Part of this research is supported by Department of Defense (DOD TATRC), USA with the project of Development of a Knowledge Base to Support Detection and Diagnosis and Research in Mammography.

Two mammogram databases: miniDDSM database and Mini-MIAS database were used in the project. The miniDDSM was down-sampled from the Digital Database for Screening Mammography (DDSM) of University of South Florida [31]. Authors in this paper wish to thank professors and scientists who created and maintained the databases for this research. Authors sincerely thank Miss Vanessa Huston for proofreading and Dr. Collin D'Souza for his help in making FROC curves.

REFERENCES

[1] H. D. Cheng, X. Cai, X. Chen, L. Hu, X. Lou, Computer-aided detection and classification of microcalcifications in mammograms: A survey, Pattern Recognition, Vol. 36, No. 12, 2003, pp. 2967-2991.

[2] L. Wei, Y. Yang, R. M. Nishikawa, Y. Jiang, A study on several machine-learning methods for classification of malignant and benign clustered microcalcifications, IEEE Transactions on Medical Imaging, Vol. 24, No. 3, 2005, pp. 371-380.

[3] A. Papadopoulos, D. I. Fotiadis, A. Likas, An automatic microcalcification detection system based on a hybrid neural network classifier, Artificial Intelligence in Medicine, Vol. 25, 2002, pp.149-167.

[4]R. Panchal, B. Verma, Neural-association of Microcalcification patterns for their reliable classification in digital mammography, International Journal of Pattern Recognition and Artificial Intelligence, Vol. 20, No. 7, 2006, pp.971-983.

[5] I. El-Naqa, Y. Yang, M. N. Wernick, N. P. Galatsanos, R. M. Nishikawa, A support vector machine approach for detection of microcalcifications, IEEE Transactions on Medical Imaging, Vol. 21, No. 12, 2002, pp.1552-1563.

[6] J. Ye, S. Zheng, C. C. Yang, SVM-based microcalcification detection in digital mammograms, Proceedings of int. conf. on computer science and software engineering 6, 2008, pp.89-92.

[7] M. Haindl, S. Mikes, G. Scarpa, Unsupervised detection of mammogram regions of interest, Lecture notes in computer science, knowledge-based intelligent information and engineering systems, Springer Berlin/Heideberg, 2010, 4694, pp. 33-40.

[8] B. W. Hong, B. S. Sohn, Segmentation of regions of interest in mammogram in a topographic approach, IEEE Transactions on Information Technology in Biomedicine, Vol. 14, 2009, pp. 129-139.

[9] D. J. Marchette, R. A. Lorey, C. E. Priebe, An analysis of local feature extraction in digital mammography, Pattern Recognition, Vol. 30, No. 9, 1997, pp.1547-1554.

[10] L. Shen, R. M. Rangayyan, J. E. L. Desautels, Application of shape analysis to mammographic calcifications, IEEE Transactions on Medical Imaging, Vol. 13, No. 2, 1994, pp. 263-274.

[11] K. J. Kim, H. W. Park, Statistical textural features for detection of microcalcifications in digital mammograms. IEEE Transactions on Medical Imaging, Vol. 18, No. 3, 1999, pp. 231-238.

[12] S. N. Yu, K. Y. Li, Y. K. Huang, Detection of microcalcifications in digital mammograms using wavelet filter and Markov random field model, Computerized Medical Imaging and Graphics, Vol. 30, No. 3, 2006, pp. 163-173.

[13] R. N. Strickland, H. II. Hahn, Wavelet transforms for detecting microcalcification in mammograms, IEEE Transactions on Medical Imaging, Vol. 15, No. 2, 1995, pp. 218-229.

[14] T. C. Wang, N. B. Karayiannis, Detection of microcalcifications in digital mammograms using wavelets. IEEE Transactions on Medical Imaging, Vol. 17, No. 4, 1998, pp. 498-509.

[15] C. B. R. Ferreira, D. L. Borges, Analysis of mammogram classification using a wavelet transform decomposition, Pattern Recognition Letters, Vol. 24, No. 7, 2003, pp. 973-982.

[16] G. Boccignone,A. Chianese, A. Picariello, Computer aided detection of microcalcifications in digital mammograms, Computers in Biology and Medicine, Vol. 30, No. 5, 2000, pp. 267-286.

[17] S. Halkiotis, T. Botsis, M. Rangoussi, Automatic detection of clustered microcalcifications in digital mammograms using mathematical morphology and neural networks, Signal Processing, Vol. 87, No. 7, 2007, pp. 1559-1568.

[18] T. Stojic, I. Reljin, B. Reljin, Adaptation of multifractal analysis to segmentation of microcalcifications in digital mammograms, Physica A, Vol. 357, 2006, pp. 494-508.

[19] D. R. Chen, R. F. Chang, C. J. Chen, M. F. Ho, S. J. Kuo, S. T. Chen, S. J. Hung, W. K. Moon, Classification of breast ultrasound images using multifractal feature, Journal of Clinical Imaging, Vol. 29, 2005, pp. 235-245.

[20] L. Bocchi, G. Coppini, J. Nori, G. Vall, Detection of single and clustered microclfications in mammograms using multifractals models and neural networks, Medical Engineer & Physics, Vol. 26, 2004, pp. 303-312.
[21] M. D. Santo, M. Molinara, F. Tortorella, M. Vento, Automatic classification of clustered microcalcifications by a multiple expert system, Pattern Recognition, Vol. 36, No. 7, 2003, pp. 1467-1477.
[22] H. D. Cheng, J. L. Wang, X. J. Shi, Microcalcification detection using fuzzy logic and scale space approaches, Pattern Recognition, Vol. 37, No. 2, 2004, pp. 363-375.
[23] M. J. Bottema, J. P. Slavotinek, Detection and classification of lobular and DCIS (small cell) microcalcifications in digital mammograms, Pattern Recognition Letters, Vol. 21, No. 13-14, 2000, pp.1209-1214.
[24] J. Xu and J. S. Tang, Detection of clustered microcalcification using an improved textual approach for computer aided breast cancer diagnosis system, CSI Communications, January 2008, pp.17-19.
[25] C. K. Chui, Wavelets: A mathematical tool for signal analysis, SIAM, Society for Industrial and Applied Mathematics, Philadelphia, 1997.
[26] M. J. Turner, J. M. Blackledge, and P. R. Andrews, Fractal geometry in digital imaging, Academic Press, 1998.
[27] P. Zhang, T. D. Bui, and C. Y. Suen, Recognition of similar objects using 2-D wavelet-fractal feature extraction, Proceedings of 16th international conference on Pattern Recognition, 2002, Quebec, Canada.
[28] D. R. Chen, R. F. Chang, C. J. Chen, M.F. Ho, S. J. Kuo, C. T. Chen, S. J. Hung, Classification of breast ultrasound images using fractal feature, Journal of Clinical Imaging, Vol. 29, 2005, pp. 235-245.
[29] E. L. Chen, P.C. Chung, C. L. Chen, H. M.Tsai, and C. I. Chang, An automatic diagnostic system for CT liver image classification, IEEE Trans Biomed Eng. Vol. 45, No. 6, 1998, pp. 783–94.
[30] R. C. Gonzalez and R. E. Woods, Digital Image Processing, 3rd version, Pearson Prentice Hall, 2008.
[31] M. Heath, K. Bowyer, D. Kopans, R. Moore and W. P. Kegelmeyer, The Digital Database for Screening Mammography, in Proceedings of the Fifth International Workshop on Digital Mammography, M.J. Yaffe, ed., 212-218, Medical Physics Publishing, 2001,ISBN 1-930524-00-5.

An Improved Iterative Watershed According to Ridge Detection for Segmentation of Metallographic Image

Jiangbo Liu and Jianxun Chen

School of Computer Science and Technology, Wuhan University of Science and Technology, P. R. China

Abstract—Metallographic images of metal crystal structures which have disconnected boundaries and heterogeneous intensity need to be segmented and analyzed to estimate the materials' performance. Comparing to other image segmentation methods, the watershed segmentation algorithm (WSA) has so far dominated in the segmentation of metallographic image based on seeds growing. However, an object in metallographic image with poor quality has more than one seed, so objects in the image will be over-segmented into several parts so that it becomes even hard to identify the segmentation result. Hence the traditional iterative watershed segmentation algorithm (TIWSA), a revised watershed algorithm, has been designed to mitigate the over-segmentation dilemma by classifying and merging pseudo-blobs to surrounding blobs. However, during the process of pseudo-blobs combination in TIWSA, a pseudo-blob may falsely be merged into a surrounding real-blob due to noises and textures in the image, so the TIWSA has to reduce combinations of pseudo-blobs in order to assure the accuracy of merging process so that the over-segmentation dilemma cannot be eradicated. Hence the TIWSA needs to be revised to protect the real-blobs and prevent them from merging other pseudo-blobs. This paper, aiming at this problem, firstly represents a new principle called *real-blob classification rule* to classify the real-blobs based on the iterative prior probability of real-blob. Once a new blob is formed, it will be examined whether it is a real-blob and all real-blobs will be recorded. Secondly, the pseudo-blob merge rule is revised that the recorded real-blobs canno longer merge other pseudo-blobs during the process of pseudo-blobs combination. The result shows that this improved TIWSA not only avoids wrong merging, but also maximizes the number of the pseudo-blobs elimination which mitigates the over-segmentation dilemma in TIWSA.

Keywords--segmentation of metallographic image, iterative watershed algorithm, ridge detection, real-blob classification.

I. Introduction

Metallography is an academic subject to study the physical structure and component of metallic materials from both macrostructure and microstructure, which is based on the photographs taken under the microscope [1]. The photographs show the distribution of metal crystal structures (MCS). Different sizes of MCSs correspond to different uses. What's more, metallic materials which have similar sizes of MCSs always have superior quality.

The statistical data and measurement of MCSs are finished by manpower all along, including area, diameter, orientation, and so on. Since the MCSs in the photograph have different shapes and sizes with irregular distribution, counting and measuring theses blobs are always heavy tasks with low precision. With the development of image segmentation, manpower can be saved by computers, using the technology of image segmentation and analysis. On the one hand, it avoids false manual operations which cause inaccurate; on the other hand, it can reduce the workload of the operators and achieve automatic process of metal casting as well. In order to realize the automation of image processing by computer, image segmentation is the first and most imperative step to identify and analyze the MCSs in the picture.

In image processing literature, the segmentation is well-studied and has been divided into several main categories [2]:

1) Threshold-based method is easy to implement and very efficient for images containing distinct objects in a contrasting background. In this algorithm, the optimum threshold separating objects and background is calculated to minimize their intra-class variance. In metallographic images, however, textures in the metal blobs lead to heterogeneous intensity of pixels in the blobs. What's more, in the process of photographing, the uneven illumination and noise make difficult for threshold-based segmentation algorithm to achieve a satisfactory result.

2) Edge-based method [3], which based on edge information, is a well-developed scheme in image processing. Since an intensity impulse often exists

Corresponding Author: Jianxun Chen , Email Address: cjxwh@wust.edu.cn

between the object and background, the edge-based method detects the impulse in a certain orientation to trace the object boundaries. However, the edges in metallographic images are often disconnected, while this method needs closed region boundaries to trace.

3) The clustering methods, for example. the K-means algorithm, choose cluster centers and assign each pixel in the image to the cluster, which minimizes the distance between the pixel and the cluster center.

4) Region growing method [4] is based on the seed growing principle. The regions are iteratively expanded by comparing all unallocated neighboring pixels to the regions. The segmentation results are dependent on the choice of seeds, so the noises in the image can lead to poor results.

5) Watershed segmentation algorithm regards the gradient scale of an image as a topographic surface. Pixels with the highest gradient magnitude intensities correspond to watershed lines, which signify the region boundaries [5]. And local minima of image gradient which mark the initial objects achieve the segmentation by region growing. However, an object in metallographic image with poor quality has more than one local gradient minimum, so every object in the metallographic image will be over-segmented into several parts. Hence the TIWSA, a revised watershed algorithm, has been designed to solve the over-segmentation dilemma by merging pseudo-blobs into surrounding blobs to improve the accuracy and the results of image partition.

To sum up, as Metallographic images have disconnected boundaries, irregular shapes and heterogeneous intensity, traditional algorithms hardly achieve effective and accurate segmentation. Comparing to other image segmentation methods, the TIWSA has dominated in segmentation of metallographic image [6], however, it cannot eliminate the over-segmentation dilemma, which still impacts the accuracy of the segmentation. This paper presents an improved TIWSA to process the real-life metallographic images.

II. Traditional Iterative Watershed Segmentation Algorithm

In order to remove the pseudo-blobs caused by over-segmentation in watershed segmentation algorithm, the TIWSA based on seed growing and ridge detection appends pseudo-blob classification and merge rules which apparently improve the exactness of segmentation.

2.1. Seed detection

In the TIWSA, the seeds which are exactly the local minima of image gradient, as the lowest water-basin which marks the initial segmentation object, achieve the segmentation by region growing. As the pixels in the MCSs are much brighter than in the boundaries, seeds can be identified automatically by double-threshold (intensity threshold and area threshold) approach. The morphological extended-maxima transform with intensity threshold is used to find the regional joined components. Holes whose area is less than the area threshold in the blob will be eliminated. As a result, a binary image after seed detection will be got which is shown in Fig. 1(b).

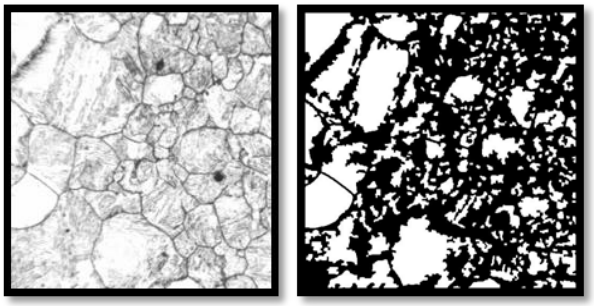

(a) (b)

Fig.1. The Seed Detection Process (a) Original image (b) Seed detection by double-threshold approach

2.2. Ridge detection

Ridge is superimposed as the highest waterline in the image at the first time watershed transform to assist the segmentation and play an essential role in pseudo-blobs classification. As the boundaries are relatively evident and robust with constant intensity (dark) and width among the cluttered MCSs in metallographic images, it is easy and efficient to utilize the ridge detection instead of edge detection for the irregular shapes and discontinuous boundaries as stated previously.

Mathematically, the ridge is defined as the local extreme point in the direction of the largest surface curvature and it can be detected by computing the eigenvalue of the Hessian matrix, which is shown in Fig. 1 (b).

Since the boundaries have larger eigenvalue of the Hessian matrix than the stripes and noises in the blobs have, ridge can be extracted by an appropriate threshold using threshold-based method which is

shown in Fig 2 (a). Finally, the ridge can be more precise after "region-open" morphological operation to

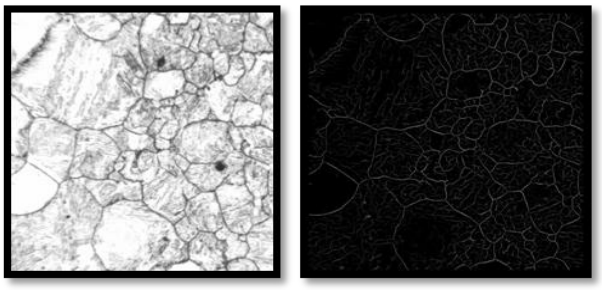

(a) (b)

Fig. 2. Ridge Detection Process (a) Original image (b) Ridge detection image by computing the eigenvalue of the Hessian matrix

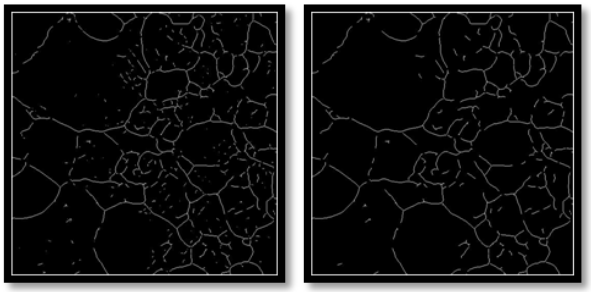

(a) (b)

Figure 3. Extract the Ridge (a) The first step of ridge extraction using threshold-based method (b) The second step of ridge extraction using "region-open" morphological operation

remove small stripes and spots caused by the noises and textures in the blobs in Figure 3(b).

2.3. Iterative Scheme

In order to solve the over-segmentation dilemma and improve the accuracy further, an iterative scheme is proposed with pseudo-blob classification rule and pseudo-blob merge rule. The first one identifies the over-segmented blob, named as pseudo-blob. The second principle reallocates the pixels of pseudo-blobs into other blobs to form integrated correct blobs, named as real-blobs [7].

2.3.1. Pseudo-blob classification rule

Define V_s as the feature vector extracted from image pixel at location $s=(x,y)$ and iteration time t. For a blob, the posterior probability of V_s from the pseudo-blob b_p or real-blob b_r respectively

$$P(b_p \mid V_s,t)=\frac{P(V_s \mid b_p,t)P(b_p \mid t)}{P(V_s \mid t)} \tag{1}$$

$$P(b_r \mid V_s,t)=\frac{P(V_s \mid b_r,t)P(b_r \mid t)}{P(V_s \mid t)} \tag{2}$$

Using the Bayes decision rule, the pixel will be classified as inside a pseudo-blob if the V_s satisfies

$$P(b_p \mid V_s,t) > P(b_r \mid V_s,t) \tag{3}$$

Be aware that the feature vector V_s associated the pixel $s=(x,y)$ is either from a real-blob or a pseudo-blob, which follows that

$$\begin{aligned} P(V_s \mid t) &= P(V_s \mid b_p,t)\times P(b_p \mid t) \\ &+ P(V_s \mid b_r,t)\times P(b_r \mid t) \end{aligned} \tag{4}$$

Taking all the pixels in a pseudo-blob into account, and substituting (1) and (4) to (3), it becomes

$$2P(b_p \mid t) > \frac{\sum_{s\in b_p} P(V_s \mid t)}{\sum_{s\in b_p} P(V_s \mid b_p,t)} \tag{5}$$

The prior probability of pseudo-blob at iteration t is updated recursively using

$$P(b_p \mid t)=\alpha P(b_p \mid t-1) \tag{6}$$

$$\alpha=\left(\frac{\alpha_0}{P(b_p \mid 0)}\right)^{1/N} \tag{7}$$

where N is the maximum number of iterations, and $P(b_p \mid N)=\alpha_0$ at the final iteration.

For simplicity, feature vector V_s is chosen as the binary ridge descriptor in this work, i.e.

$$P(V_s \mid t)=\begin{cases} 1 & s=ridge \\ 0 & s\neq ridge \end{cases} \tag{8}$$

2.3.2. Pseudo-blob merge rule

There are two basic rules to regroup the pixels inside a pseudo-blob which are pixel-by-pixel and all pixels as a whole. In this work, the later one always gives reasonable results. Therefore, the proposed merge rule is based on "winner-take-all" principle.

(1) Label the pixels inside pseudo-blobs as blank.
(2) Re-watershed the blank in the image to let the surrounding blobs encroach the pseudo-blob pixels.
(3) Count the pixels encroached by the surrounding blobs and compute the rate. The surrounding blob which has the biggest rate will be the winner.

(4) Assign the winner's label to all pseudo-blob pixels.

2.4. The drawbacks of TIWSA in application

The prior probability of pseudo-blob is a fundamental parameter in the iterative scheme that can mitigate the over-segmentation dilemma, as the pseudo-blobs are identified and merged based on this parameter. Whereas when it continuously grows, the TIWSA may erroneously merge a pseudo-blob into a nearby real-blob because the noises and the blob textures in metallographic photographs impact the processes of pseudo-blobs identification and re-watershed. Hence we have to reduce this parameter to a proper size using the TIWSA in order to guarantee the real-blobs, although reducing this parameter will left some pseudo-blobs in the image.

III. Improved Iterative Watershed Segmentation Algorithm

To get rid of the drawbacks of TIWSA mentioned above and promote the accuracy of partition, this paper proposes a new principle called the real-blob classification rule and the pseudo-blob merge rule is revised according to the proposed rule.

3.1 Real-blob Classification Rule

The Real-blob has already had a correct form, thus any combination with other pseudo-blobs will destroy its correct shape and boundary. Similar to pseudo-blob, the real-blob is identified by the prior probability of real-blob which is computed as follow:

V_s is the feature vector extracted from image pixel at location $s=(x,y)$ and iteration time t. Using the Bayes decision rule, the pixel will be classified as inside a real-blob if the V_s satisfies

$$P(b_r \mid V_s,t) > P(b_p \mid V_s,t) \tag{9}$$

Substituting (2.2) and (2.4) to (3.1), it becomes

$$2P(b_r \mid t) > \frac{\sum_{s\in b_r} P(V_s \mid t)}{\sum_{s\in b_r} P(V_s \mid b_r,t)} \tag{10}$$

The prior probability of real-blob at iteration t is updated recursively using

$$P(b_r \mid t) = \beta P(b_r \mid t-1) \tag{11}$$

$$\beta = \left(\frac{\beta_0}{P(b_r \mid 0)} \right)^{1/N} \tag{12}$$

where N is the maximum number of iterations, and $P(b_r \mid N) = \beta_0$.

In order to prevent omitting any of the real-blobs, once a new blob is generated after merging a pseudo-blob, it has to be examined whether it is a real-blob. All identified real-blobs are recorded and used in the pseudo-blobs merge rule.

3.2 Revised Pseudo-blob Merge Rule

The new real-blob after identified will be protected and can no more merge other blob during the merge process. As a result, the original pseudo-blob merge rule is revised as follow:

(1) Label the pixels inside pseudo-blobs as blank.
(2) Re-watershed the blank in the image to let the surrounding blobs encroach the pseudo-blob pixels.
(3) Count the pixels encroached by the surrounding blobs and compute the rate. The surrounding non-real-blob with the biggest rate will be the winner. If the surrounding blobs are all real-blobs, the real-blob with the least prior probability will be the winner.
(4) Assign the winner's label to all pseudo-blob pixels.

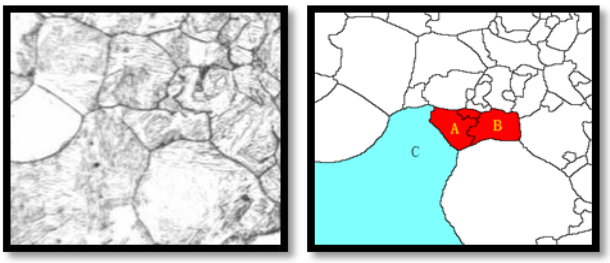

(a) (b)

Fig. 4. Before Combining the Pseudo-blobs (a) Original image (b) one step before a combination of pseudo-blobs

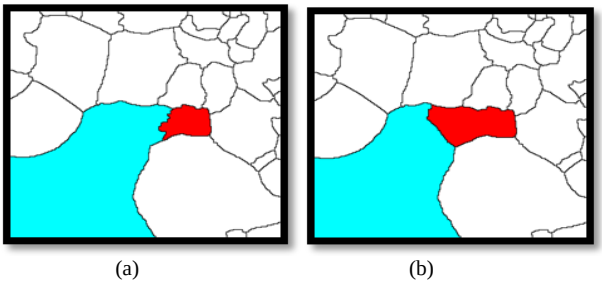

(a) (b)

Fig.5. The Different results of TIWSA and IIWSA After Combining the Pseudo-blobs (a) Result of TIWSA (b) Result of IIWSA

3.3. New Rules in Application

Fig. 4 shows a result of new rule in application of metallographic image segmentation. Fig. 4 (b) is one step during the iterative watershed segmentation of a metallographic image which is shown in Fig.4 (a). Compared with original photograph, the red pseudo-blob A in Fig. 4(b) should be merged to the red blob B. The blue blob C has been a real-blob. However, C in the original photograph has numerous textures which make C much easier than B to encroach the pseudo-blob A. Hence after the re-watershed, as shown in Fig. 5(b), C, instead of B, is the winner and merges the blob A as it occupies the biggest rate of A.

Then we add the real-blob classification rule ($P(b_r \mid N) = \beta_0 = 0.8$) to prevent real-blob C from combining the pseudo-blob A. As the result shown in Fig. 5 (b), blob B merges the blob A and forms a new real-blob leaving real-blob C unchanged. The result shows that once the real-blobs are formed, they can remain unchanged during the merge process. Hence, the prior probability of pseudo-blob can be raised to merge more pseudo-blobs caused by over-segmentation dilemma.

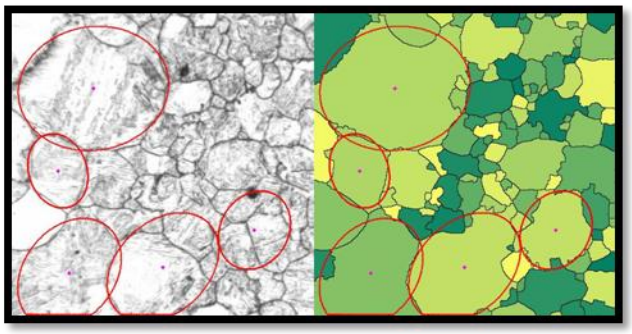

(a)

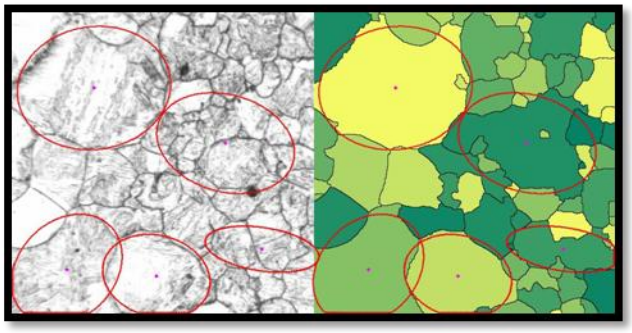

(b)

Fig. 6. The Comparison of the Results in Application Using TIWSA and IIWSA (a) Result using TIWSA (b) Result using IIWSA

IV. RESULTS AND ANALYZES

This section shows the comparison of the results between TIWSA and IIWSA. Fig. 6 (a) is the result of TIWSA($P(b_p \mid N) = \alpha_0 = 0.4$, $P(b_p \mid 0) = 0.1$) comparing with the result of IIWSA ($P(b_p \mid N) = \alpha_0 = 0.62$, $P(b_p \mid 0) = 0.1$, $P(b_r \mid N) = \beta_0 = 0.68$) in Fig. 6 (b). Evidently, the IIWSA offers a more precise segmentation result than TIWSA, in which more pseudo-blobs become new real-blobs and the real-blobs remain correct after they are formed.

Fig. 7 and Fig. 8 are the results comparing with the original images of other metallographic images using IIWSA. Although these metallographic images have poor quality with disconnected boundaries and heterogeneous intensity which still affect the result of segmentation, most blobs are well segmented according to the original images. In addition, every blob is modeled as ellipse [1] with parameters, for instance, centroid, major/minor axis, orientation, and so on. And 5 blobs which have largest area are marked with red ellipses on both original and segmented image for highlighting.

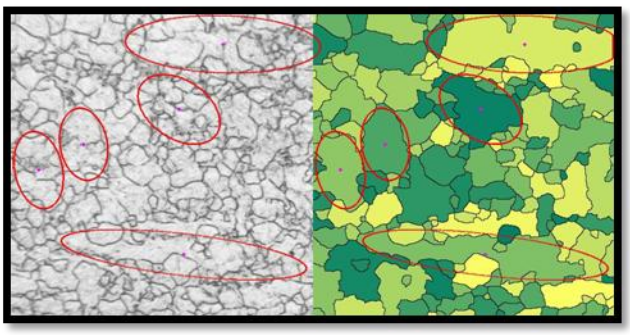

Fig. 7. An Application in Another Metallographic Image (1)

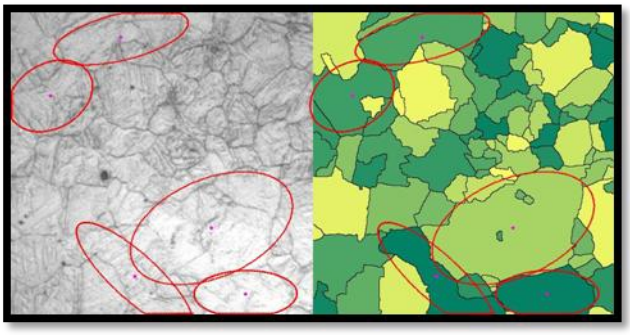

Fig. 8. An Application in Another Metallographic Image (2)

V. CONCLUSION

This paper proposes a revised image segmentation algorithm that mitigates the over-segmentation dilemma of traditional iterative watershed segmentation algorithm by adding a real-blob classification rule and revising the pseudo-blob merge rule. The method can handle complex objects with irregular shapes, disconnected boundaries and heterogeneous intensity. The computational cost is relatively a bit high compared with TIWSA. However, it offers a more satisfactory result. This revised algorithm can be efficiently used not only in metallographic images, but also in other areas, such as medical applications.

Further research will be conducted by adding new processes and principles to tackle more texture disturbance and optimizing the algorithm in order to diminish the computational cost. To inspire further studies on this potential field, the source code could be downloaded freely from Matlab Central.

REFERENCE

[1] Li Chen, Min Jiang, and JianXun Chen, "Image Segmentation Using Iterative Watersheding Plus Ridge Detection", 2009 IEEE International Conference on Image Processing, iro, Egypt, Saturday, November 7 - Tuesday, November 10, 2009.

[2] D. L. Pham, C.Y. Xu, and J. L. Prince, “Current methods in medical image segmentation,” Annual Review of Biomedical Engineering, vol. 2, pp. 315-337, 2000.

[3] L. S. Davis, “A survey of edge detection techniques”, Comput. Graphics and Image Processing, vol. 4, No. 3, pp. 179-205, 1975.

[4] S. W. Zucker, “Region growing: Childhood and adolescence”, Comput. Graphics and Image Processing, vol. 5, No. 3, pp. 382-399, 1976.

[5] Hill, P.R., Canagarajah, C.N., Bull, D.R., “Image segmentation using a texture gradient based watershed transform,” IEEE Transactions on Image Processing, vol. 12, No. 12, pp. 1618-1633, 2003.

[6] Meyer, and Fernand, “Topographic distance and watershed lines,” Signal Processing, vol. 38, No. 1, pp. 113-125, July 1994.

[7] A.Sri Nagesh, Dr.G.P.S.Varma, and Dr A Govardhan, "An Improved Iterative Watershed and Morphological Transformation Techniques for Segmentation of Microarray Images," Computer Aided Soft Computing Techniques for Imaging and Biomedical Application, vol. CASCT, No. 2, pp. 77-87, 2010.

The Use of Geospatial Information Systems in the Analysis of Pollution Trends in Southern Mississippi Region

Edmund C.Merem[a], Yaw.A.Twumasi[b], Sudha.Yerramilli[c], Chandra Richardson[a]

[a] Department of Urban and Regional Planning, Jackson State University, Jackson, MS 39211, USA
[b]Department of Agriculture Research Unit, Alcorn State University, Lorman, MS 39096, USA
[c] National Center for Biodefense Communications, Jackson State University, Jackson, MS, 39204, USA

Abstract –In the last several decades, many cities in the United States continue to face the menace of environmental pollution at an alarming proportion with little use of geospatial technology and appropriate methods in dealing with the problem. The perverse nature of the problem not only threatens the different life forms in the environment, but it diminishes ecosystem quality and the livability of cities. While society tries to use policy to internalize externalities through taxes or prohibition, pollutants remain the most conspicuous examples of negative externalities. Compounding the matter is the absence of suitable tools such as Geographic Information Systems (GIS) for tracking the spatial dispersion of the quantity of pollutants and their impacts so that cities can have a better insight of the problems posed to their environment. At the same time, many cities lack complete inventory on the state of the environment in their areas. Apart from few studies, very little has been done to address the problem. The purpose of this study is to analyze the state of pollution and mapping of the trends within cities in the Southern Mississippi region of the United States. Emphasis is on the problems of air pollution, the source and the amount of pollutants, the consequences and the remedies. In terms of methodology, the paper uses descriptive statistics, correlation analysis and GIS to analyze the state of the environment and stressors within cities. While the results show that pollution activities have proliferated over the years in the region due to the growing presence of environmental stressors. A temporal spatial analysis using GIS to map the widespread discharge of chemical contaminants revealed a gradual spreading of stressors with risks to the sensitive coastal ecosystem. In the context of the region, GIS provides decision makers the capability for locating the quantity of pollutants and their impacts. The paper suggests the need for governments to enforce air quality standards and the adoption of methods for reaching those standards.

Key Words –GIS, pollution, pollutants, southern Mississippi, region, environment, remedies

I. Introduction

In the last several decades, many cities in United States including those in the Southern Mississippi Gulf coast region continue to face the menace of environmental pollution at an alarming proportion with little use of geospatial technology and appropriate methods in dealing with the problem. Taking a cue from Dennison (2007) notion of coastal environments as regions of strong gradients and major human impacts, the Southern Mississippi region has not only been sprawling with major developments but there are concerns as to whether the increased growth is impeding the region's air quality and the environment. In the area, pollution sources from the petro-chemical sector, power, and the agricultural industry operate within the vicinity of sensitive estuarine environments and metro areas inhabited by large populations.

Considering the severity of the ensuing impacts, most of the counties in the region rank highly nationally as some of the dirtiest in terms of environmental quality.

The perverse nature of the problem not only threatens the different life forms in the environment, but it diminishes the ecosystem quality and the livability of cities. This has created a situation whereby life support systems in the ecosystem are exposed to danger. Due to these anomalies, it is not surprising that governments have resorted to different types of policy instruments for a better management of natural resources (Doern, 1974). In the environmental field a vast majority of instruments under consideration include regulation, market or economic based incentives, voluntary mechanisms, permits, subsidies and taxation. Regulatory instruments are tools used by governments to control the activities of polluters through the enforcement of stricter standards during the process of production. While policy makers require industries to internalize environmental externalities through the imposition of taxes or prohibition and the use of polluter pay principles, pollutants remain the most conspicuous examples of negative externalities in areas such as the southern Mississippi region and other places.

Corresponding Author: Edmund C. Merem, Email Address: Edmund.c.merem@jsums.edu

Compounding the matter is the absence of suitable tools such as GIS for locating and appraising the quantity of pollutants and their impacts so that cities such as those in Southern Mississippi can have a better insight of the problems posed to their environment. Considering that many of those cities lack complete geospatial inventory on the state of the environment in their areas coupled with paucity of studies, very little has been done to address the problem. To overcome these difficulties, GIS has emerged as a vital tool for integrating geo-referenced data on pollution assessment. It is also a spatial system for the organization, storage, transformation, retrieval and analysis of data where location is important (DeMers, 1997; Aronoff, 1989). In fact, quite a number of GIS oriented approaches for forecasting the dispersion of chemicals are widespread in the literature (Schwetz et al., 1991).

Just as the visualization of pollution patterns in a map has now been optimized in the arena of public environmental health through GIS (Jerret, 2001), the capability to map pollution hazards geographically offers decision makers better clues on where to focus abatement measures. In addition to mapping externalities (Miller, 2001), decision makers can use the device to plot potential predictors and environmental quality inhibitors. Accordingly, several studies have mapped pollution concentrations (Burnnet et al., 2001, Jarrett 2001, Pikhart et al,. 1991, 2001); and socio-economic distributions of pollutants (Buzzelli et al., 2003; Jareet 2001. The spatial representation of pollution predictors in public policy helps one decide on target locations and the mechanisms for monitoring the outbreak of disasters. For more information on other researchers who integrated GIS with spatial statistics, see the work of Gatrell and Loytonnen (1998); and Jerrett et al. (2001). In light of these observations, part of the emphasis in various sections of the paper involves the mapping of potential stressors and pollution predictors in the study area.

II. Objectives and Organization

The purpose of this study is to analyze the state of pollution and mapping of the trends within cities in the Southern Mississippi region of the United States. Emphasis is on the problem of air pollution, the source and amount of pollutants, and ways of attaining environmental quality. In terms of methodology, the paper uses descriptive statistics, correlation analysis and GIS to analyze the state of the environment and stressors within cities. There is also an attempt to design a geospatial methodology for assessing the extent and location of pollutants and their quantity in the study area. The paper is divided in four parts. Part one covers the introduction and the background information with focus on the issues. The second part describes the study area and the methods. In part three, the results of temporal spatial data analysis highlighting the extent of environmental pollution are presented along with a geospatial analysis of the patterns of pollution dispersion in various locations. Part four offers a brief discussion of the findings with some lines of action for attaining pollution abatement and a concluding statement.

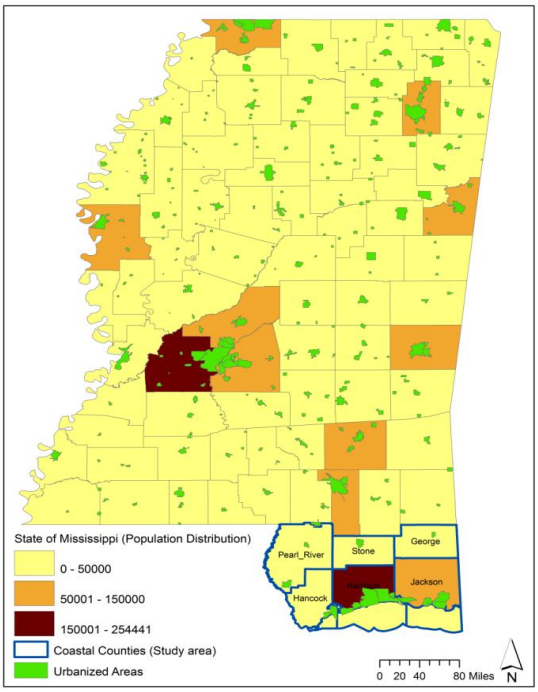

Fig. 1. The Study Area: Southern Mississippi region

III. Methods and Study Area

The study area located in Southern Mississippi along the coastal plains in the Southern portion of the map in Fig. 1 encompasses 6 selected counties. The map shows the state of Mississippi with population distribution of different levels and the spatial location of the urban areas and the delineation of coastal counties within the study area. The six counties under analysis consisting of Pearl River, George, Stone, Harrison, Hancock and Jackson have a combined population 437,408 in 2006 (Table 1). In recent years, three of the coastal counties of Southern Mississippi have experienced significant growth. In fact between 1950 through 1990, Hancock, Harrison and Jackson counties had a population growth of 168%, 96% and

276% respectively while George and Pearl River Counties each gained between 65% and 90%.

The study location which stretches through major urban areas along the Gulf coast region of Pascagoula and Biloxi-Gulfport metro areas shown in the Table, contains major thriving urban areas prone to severe pollution and other environmental problems. The major river basin, the Pascagoula is Mississippi's second largest basin measuring approximately 164 miles long and 84 miles wide. While, the basin drains an area of about 9,600 miles before emptying into the Gulf of Mexico. The Pascagoula is also the largest unimpeded major river system in continental United States. The major streams in the area include the Pascagoula, Leaf and Chickasawhay Rivers as well as the Black and Red Creeks (MDEQ and NRCS 2007). The total estimated land area of the watershed measures about 386,008 acres with non-irrigated cropland and pastureland as the major land-uses. About 72% of the basin contains forested area while the other 21% is classified as agricultural land.

With the presence of generally well-drained and moderately drained soil types, the basin contains about 542 farms and an average farm size of 94 acres. The size of cropland stretches across an area estimated at 22,100l acres coupled with an additional 20,800 total acres devoted to pastureland (NRCS 2007).

From an economic standpoint, timber use in the basin generates $325 million dollars to the economy. The Pascagoula basin produces 75% of oil and gas production in the state and there are about 250 surface mining operations in the area (Estes, 2006). With the recurring declines in agriculture and timber activities in the region in recent years, other forms of land use have increased their impact on the ecosystem. Although in channel mining was quite rampant in the area until it was banned in 1995. Floodplain sand and gravel mining remain active on the Bowie river side of the basin, as well as Thompson creek and Leaf River. During the same period, simultaneous development has been occurring in many parts of the basin, including the cities of Pascagoula, Moss Point, Meridian, Hattiesburg and Laurel (Mossa and Cooley, 2005; Estes, 2006).

Methods Used

This paper stresses a mix scale approach involving the use of descriptive statistics, and geospatial technologies of GIS in processing data provided through government sources and data bases from other organizations. This research also presents a methodology designed for use in situations where physical accounts, descriptive statistics and GIS analysis of the state of the environment within cities are not readily available. The raw spatial data made up of maps and other kinds of digital information used in the research came from the United States Geological Surveys (USGS) data procurement unit, the USDA and the US Environmental Protection Agency (EPA), the Government of Mississippi, the United States Census Bureau and other organizations such as the University of Maryland On line data unit.

Step 1: Data Acquisition

The first step involves the identification of the variables needed to assess the state of pollution among cities in the Southern Mississippi region of the United States. The spatial units of analysis consisted of the counties located in the Gulf region (Table1). The variables encompasses environmental data such as land cover elements (of the amount of fertilized farmland areas, impaired water bodies,) environmental releases from air, water, land, underground injection of pollutants, offsite transfer of pollutants and produced wastes. Others include pollution sources, their quantities and various miscellaneous pollution indicators (see Appendix). This process continued with the design of data matrices covering the various periods from the 1980s, 2000 and beyond.

In addition, to the design stage, access to databases and abstracts that are presently available within the Federal and state archives in Mississippi and the United States Geological Surveys (USGS), the United States National Aeronautical and Space Agency (NASA) and host of other entities quickened the search process. The spatial data was acquired from the USGS and the Mississippi Automated Resources Information System (MARIS). The Information obtained covered the Southern Mississippi region of Pascagoula-Biloxi Gulfport area for the separate periods of 1988 and 2004.

Step 2: Geo Spatial Data Acquisition and Processing

For the study area of Southern Mississippi region, multi-temporal spatial data made up of shape files and maps were obtained for the study. The data that were assembled for the Southern Mississippi urban counties of Stone, Pearl River, Harrison, Hancock, George, and Jackson include pollution emission and ecological data. Others include shape files, paper and digital maps between 1988 through 2004. All the spatial and

temporal data were analyzed using ARCVIEW and SPSS. The outputs ranged from texts, tables and maps as well as matrices.

The processed data displayed under different legends makes ecological variables like water, impaired areas and others appear as shades of blue and brighter reds indicating impaired watersheds while the other pollution emission indicators were distinguished in different colors as well. Furthermore, the output was visually compared with the trends evidenced in the area to see the extent of spatial dispersion across time and space along the tributaries of the Southern Mississippi Gulf coast environment. The remaining procedure involves spatial analysis and output (maps-tables-text) covering the study period using ARCVIEW GIS. This process helped show the extent of temporal-spatial evolution of environmental pollution predictors induced by industrial and development activities. This provided opportunities to undertake the sequential mappings of the stressors and pollutants impacting the stream environments of the South Mississippi region.

IV. Environmental Pollution Analysis

This part of the paper presents the results of the descriptive statistics and temporal-spatial analysis of pollution trends using GIS and correlation analysis on a set of indicators associated with environmental pollutants already outlined in the methodology. The effort here consists of the snapshot on a wide range of information focusing on various pollutants, fertilized areas and impaired waters and other variables in the region.

Temporal Analysis of the Nature of Environmental Toxics

At Pearl River County during the 12 year period of 1988 and 2002, the quantity of air pollutants discharged into the atmosphere by industries stood at 1,1903,364 pounds. Among the other indicators, the volume of total environmental releases, offsite transfers and total production of related wastes amounted to 1,211,356, 634,464 and 4,561,438 pounds during the same periods. Within the individual periods, the quantity of total environmental releases of pollutants estimated at hundreds of thousands of pounds reached significant levels during 1990 and 1992. Similar pattern of releases in the county consists of 244,116 in 1990, 229,101 by 1991, 129,386 in 1992 and 99,812 pounds in 1993. This was followed by additional pollutants estimated in tens of thousands that appeared from 1993 and 2002. In terms of pollutants from off sites, the largest transfers into the county occurred in 1992 and 1997 when the volumes ranged from 467,050 and 108,338 pounds respectively. The total production of related wastes not only reached the million mark of 1, 093, 397 in 1991, but it intensified further in the county with more wastes estimated in tens of hundreds of thousand pounds during the ensuing 11 years from 1992 -2002 (Table 2). George County as the table indicates seem to have negligible levels of pollutant releases when tallied and compared with the other counties (Table 3). As a result, there would be no extensive analysis of the trends in the county.

Between 1988 through 2002 at Stone county, the overall tally in the various categories of pollution indicators for the area consists of 193,486 pounds for air alone and about 195,233 pounds for combined environmental releases into air land and water. Among the other pollution categories, about 124,535 pounds came from offsite transfers while total production related wastes accounted for 335,956 pounds. In Stone county, the total discharge of environmental toxics were amazingly high between 1990 -1994 when the largest releases into the atmosphere ranged from 36,033 to 35,043 during 1990 through 1991. The volume of pollutants that were discharged in the air in the later years consists of 11,980 pounds in 1999, 13,066 in 2000, 14,740 in 2001 and 7,532 in 2002. At the same time, the total offsite transfers of pollutants which reached significant levels were in the order of 30,625, 32,384, and 34,793 in 2000, 2001 and 2002 respectively.

In the county, production related wastes varied from 38,896 in 1991, 28,406 by 1992 and 21,887 in 1994. In the later years, the fiscal year 2001 with 78,195 pounds emerged as the period stone county had more total production related wastes than ever. Even though the quantity of contaminants for the county was tallied in thousands of pounds, they were still lethal enough to inflict irreversible harm on the ecosystem and the residents of the area (Table 4).

For Harrison County as Table 5 shows, the volume of contaminants in the area appeared much higher than some of the other areas in the region. Note that in the county between 1988-2002, when the overall total from air releases was estimated at 84,761,839 pounds, about 375,269,624 pounds of pollutants were injected into the underground. With the sum of all environmental releases including the former and later categories estimated at 467,742,535 pounds, the quantity of offsite transfers and production of related wastes stayed at 6,379,769 and 431,514,796 pounds respectively. The quantity of pollutants in all the

categories appeared in tens of millions from 1988 and 2002. While air releases ranged from 11,034,704 and 12,384,227 between 1999 and 2000, additional volumes of large releases in millions consists of 2,200,000 from land in 1988 and over 1 million pounds of land releases from the period 2000 through 2001. Note that the quantity of underground injection of toxins were initially all in tens of millions of pounds, but as time went on during 1988-1994 period, the county eventually emerged with far more larger volumes of toxins estimated at 40, 500,000 and 57,000,000 pounds.

In a similar vein, the total environmental releases for Harrison County reached its biggest level of 60,324,170 pounds during the 1994 fiscal year at a scale that surpasses the entire periods. In addition, to this, two offsite transfers measured at 1,136,491 pounds, and 1,215,912 occurred in both 1994, and 1997 while the quantity of the rest of the transfers in the remaining years of 1988-2002 stayed under hundreds of thousands. Production related wastes in high tens of millions were evident during 1991-1994 and all through 1997 to 2002 when the volumes were in the mid tens of millions. In this period, the largest volumes of produced waste were in the order of over 67,000,000 in 1992 to 1994 along with 51,752, 479 pounds that was audited in 1991 (Table 5) .

Hancock County in the various years was exposed to about 2,028,564 pounds in air pollutants, when tallied with the amount of toxics ravaging land and water, the total number came to 2,041,579 for the overall environmental releases. For the remaining indicators, as` the county took in 8,864,117 pounds from offsite transfers, production related wastes totalled 283, 873, 460 pounds from 1988-2002. In terms of the brake down among the individual years, the total environmental releases which appeared in hundreds of thousands came in the order of 707,554, 549,355, 204,610, and 101,509 pounds in 1988, 1989, 1990, and 2001. Even though the total offsite transfers in hundreds of thousands of pounds occurred at a higher frequency in the county between 1988-2001, the amount that the county received in the fiscal years of 1997 and 2002 still ranked higher at 1,386, 500 and 1,084,723 pounds respectively. From the Table see also that the total number of production wastes in the low millions were not only quite pronounced, but the county contained huge chunks of industrial garbage estimated between 48,447, 102 to over 75,000, 000 pounds in 1999, 2000, 2001, and 2002 (Table 6).

Turning to the county of Jackson, the table indicates large levels of contaminants with 59,453,969 pounds in overall volume of air release, 5,334,626 for water, and 5,769,513 in land toxics. Among these categories, about 5, 09,587 pounds are attributed to underground of injection of pollutants. With the entire environmental releases estimated at 71,067, 693, the county took in additional 257,458, 702 pounds from off site transfers while the industries were responsible for an estimated 1500, 677,084 pounds of waste. In each category of the indicators from air releases to underground injection of toxics, the county experienced colossal discharge of pollutants between 1988 through 2002. In as much as the total environmental releases during the 1988-2000 period seemed stable, those in the low or 1 millions occurred in 1989-1994 as environmental release measuring over 4 million pounds appeared more in 1990, 1988, 1992, 1993, and 1995.

The other evidence of this trend includes the volume of toxics estimated at 4,643,321, 4,858,459, and 6,394,074 in 1997, 1998 and 2000. The largest volumes consist of 5,466,125 and 5,443,863 that were produced in 1991 and 1996. In the later years of 2000 -2001, the total releases jumped to 6,394,214, and 6,280,962 pounds. Within this period, total off site transfers of pollutants in 1993 estimated in millions at 192,706,725 surpassed the other ones as the largest in that category. See also that in 1993-1998, when the total production waste were tallied in hundreds of millions, the 313, 088,808, and 204, 362, 692 pounds in waste streams in 1992 and 1998 exceeded those of the other periods under analysis (Table 7).

Fertilized Acreages of Agricultural land, Impaired Water Areas and List of Pollution Sources

In terms of the size of acreages of land treated with fertilizer, the counties of Pearl River and George appear to have exceeded the other areas in the use of fertilizer nutrients. The use of fertilizers in Pearl River ranged from about 32,262 acres in 1992, 28,907 during 1997 and 14,234 by 2002. Over the years (1992, 1997, and 2004) at George County, the area of agricultural land treated with fertilizer was estimated at 16,484, 11,907 and 19,395 acres. Within the same periods at Stone county, fertilizer acreages consists of 8,846 in 1992, 8,671 in 1997 and 8,886 in 2002. In 1992 about 3,530 acres were under the direct applications of fertilizer nutrients in Harrison County, in the following periods of 1997 and 2002, the size of fertilized areas stayed somewhat identical at 4,514 in 2002 and 4,323 in 2002. For Hancock County, land treated with fertilizers was estimated at 6,135 acres in 1992, 9,271

by 1997 and 7,062 during 2002. Between 1992, 1997 and 2002 in the Jackson county area, the numbers varied from 3,511 to 11,832 and 8,779 respectively (Table 2).

On the percentages of change, see that the counties were evenly split in terms of declines and gains in 1992 -1997. In fact, three counties (Harrison, Hancock and Jackson) made gains while three other areas most notably Pearl River, George and Stone and others saw their acreages of fertilized land decline. The breakdown of the figures showed that fertilized areas grew by 27 % at Harrison, 51% at Hancock and by 238 % in Jackson County. With the exception of the 62 % gains in fertilized areas for George and 2.4% for Stone county, the remaining four other counties experienced sizable declines in the period of 2002 through 2004 (Table 8).

On the other environmental variables, in 1998 impaired water areas appeared more in the South Mississippi urban areas with the three counties of Pearl River, Harrison, and Hancock each accounting for the 2 major water areas under impairment. In the same period, George and Jackson counties led the rest of the region with 5 impaired water areas while Stone emerged as the county with the least impaired water surface. Among the counties, in 2002 and 2004, only the George county and Hancock areas experienced water surface impairment in 2 areas while the rest had either one case of reported impaired surface or none at all (Table 8). From the list of pollution sources, as Tables 9 indicates, Jackson County, Harrison, Hancock and Stone appeared to have more pollution sources from various industries including petrochemical, mining power and utility companies. Among the counties, Jackson ranks 1st with 10 pollution sources or facilities, followed by Harrison at 2nd with 7 sources. Others include Hancock listed at 3rd with 4. The two other counties of Pearl River and Stone each had 3 sources while George county finishes with just only 2 (Tables 9).

V. Correlation Analysis

To buttress, linkages to the behavior of some of the variables herein analyzed in contributing to stream habitat pollution, the simple correlation analysis performed on selected variables shows a positive relation between impaired waters and fertilized acres. With this increase in fertilized acres, there came a major rise in the number of impaired waters as well.

Spatial analysis on some of the indicators

Turning to the level and severity of pollution in the region, see that the classes as represented in fig. 2 consist of four types such as highly polluted, polluted, moderately clean and clean up to 50. In terms of definition, highly polluted refers to areas on the map that experienced extreme forms of contamination while polluted denotes normal forms of it. Moderately clean and the clan classes on the map represent areas that experienced fairly and normal levels of cleanliness.

During the fiscal year of 2002, the geographic diffusion of pollution appeared highly pronounced in the coastal counties of Jackson, Harrison and Hancock. From the map, both Jackson and Harrison share similar clusters as the mostly highly polluted areas while Hancock emerged as a polluted county as well (Fig. 2).

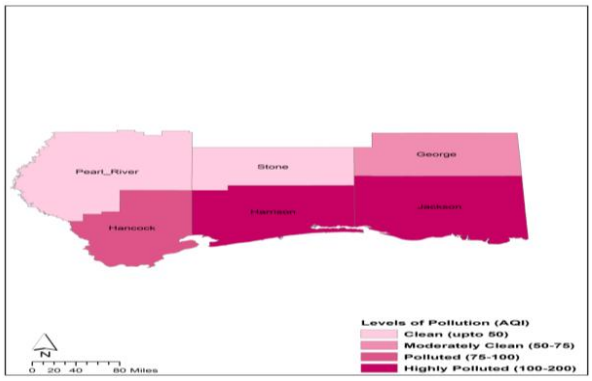

Fig. 2. Levels of Pollution 2002

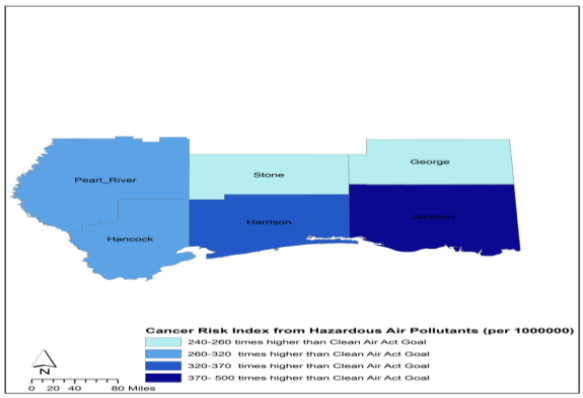

Fig. 3. Cancer risks from Hazardous air pollutants 2002

Pertaining to case risks from hazardous air pollutants represented in Fig. 3, the first classes (370-500 times and 330-370 times) refers to areas that were 300 -550 higher than the policy goals and threshold as required by the provisions of the US Clean air act. The same can be said of the second set of classes represented in the listed categories of 300-

320 and 240-280. These are areas where the intensity of pollutants exceeded the permissible levels under the US Clean Air Act in terms of air quality. Even though the average individual added cancer risks from hazardous air pollutants are somewhat even, in 2002 among the counties, those around the coast and the lower part of the study area such as Jackson, Harrison, Hancock as well as Pearl River still ranked relatively higher in terms of risks per million in the region at levels much higher than the US Clean Air Act goals (Fig. 3).

In a place where percent changes in Toxic Release Inventory (TRI) release provides clues on the state of the environment, Fig. 4 helps identify the severity and the levels between 1988 to 2002 by showcasing the four different classes. The initial class of > 100% increases in TRI represents areas where the percentile level rose significantly by over 100%, while the 50-100 % increase in TRI release class refers to places on the map where they are only under 100% or medium. Note also the presence of the no change category involving the releases at a constant level followed by the over > 100 decrease category in which the release of TRI is in decline. The percentage of changes in the amount of TRI chemical releases between 1988-2002 shows a concentration of both high and medium (100 % > to 50-100%) increases clustered around the upper counties of George, Stone and Pearl River and alongside the coastal area of Jackson County. Under this indicator, the areas in the region classified as having high or 100 percent decreases in the chemical releases appear scattered in different patches around Harrison and Hancock counties (Fig. 4). The percent of surface water with reported problems with its four classes can be distinguished by the > 90% category representing impaired waters experiencing sizeable damages. There also those with damages classified under the 80-90% range along with 60-80% and < 60% levels of damages. The percentage of surface water in 2002 with reported pollution problems along the watersheds in the study area seemed rampant at various scales ranging from 60-90% and over (Fig. 5). With much of the problems concentrated in Stone and Harrison counties with 90% and over of the watersheds involved, Pearl River and Hancock counties on the other hand, also faced similar threats on 80 to 90% of their watersheds.

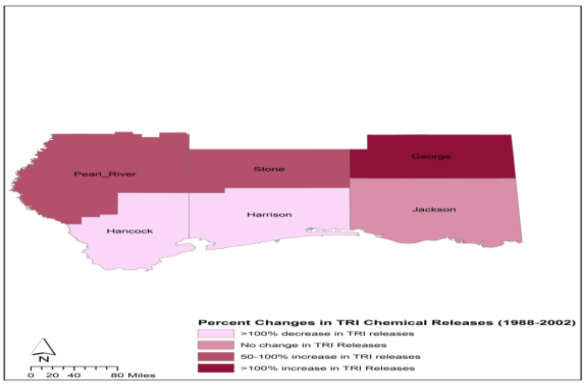

Fig. 4. Percent Changes in TRI releases (1988-2002)

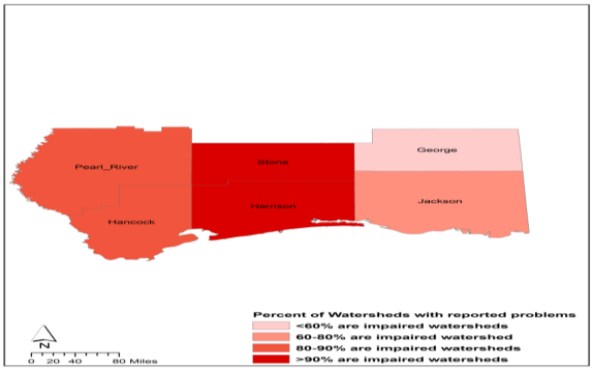

Fig. 5 Percent of surface waters with reported problems 2002

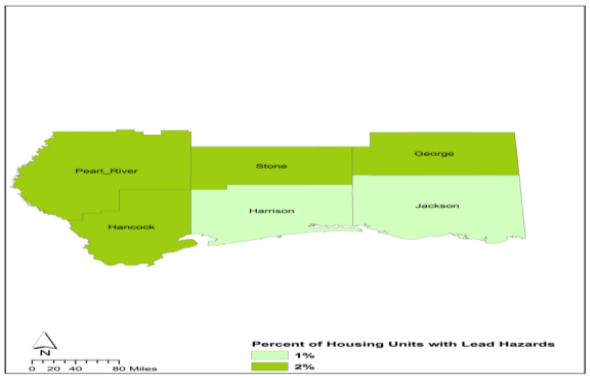

Fig. 6 Percent of housing units with lead hazards 2002

The percentage of housing units exposed to high risks of lead hazards in 2002 are defined by the 1% to 2% levels, with the later exceeding the former in the percentage category. Note that those presumed to be in the top 2 percent category seemed fully concentrated in 4 of the six counties mostly in the upper and lower part of the map. The exceptions are the counties of Harrison and Jackson both of which had 1 percent of their housing units under exposure to lead hazards (Fig. 6). The number of Toxic Release Inventory sites defined by four classes contains 7-10 group of TRI sites ranked as the highest numbers. This is followed

by the medium types represented by 4-6 sites. The lower end of the TRI sites represents those having 2-3 and 1 TRI sites alone. In 2002, when large numbers of toxic release inventory sites were located in the various counties, Jackson County emerged with more sites (7-10) alongside the county of Harrison which had 4-6 of those sites. In the same period, the number of toxic release inventory sites in the other counties stood at 1-3.

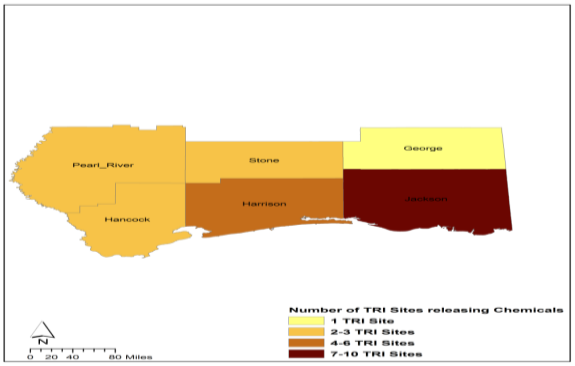

Fig. 7 Number of TRI sites releasing chemicals 2002

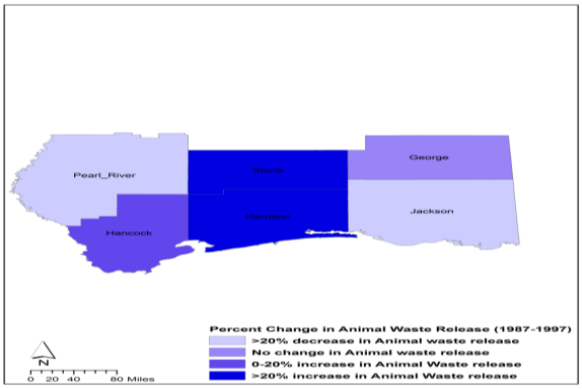

Fig. 8 Percent change in release of Animal waste (1987-1997)

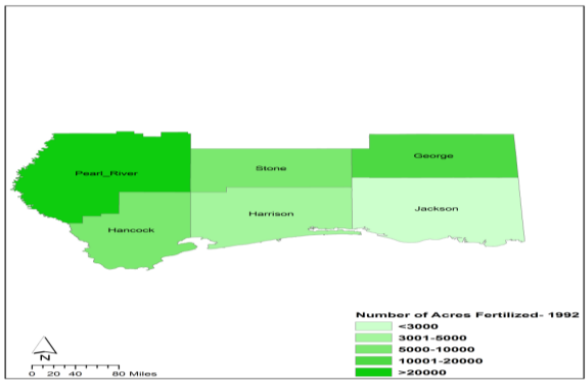

Fig. 9 Number of Acres Fertilized 1992

Pertaining to the spatial tracking of animal waste release in Fig. 8, it is defined by four classes of >20% increase and 0-20% increase in animal waste, no change in animal waste release and <20% decrease in animal waste release. The > 20% and 0-20% increase in animal waste stands as a measure of the high and medium rises in those two categories over time. The no change class refers to no variations while the <20% decrease in animal waste release stands for the extent of declines. See that the high, medium and low percent increases were evident in Stone, Harrison and Hancock counties with no changes in George County. Note also the decreases in animal waste release evident in Pearl River and Jackson counties between1987-1997 (Fig. 8).

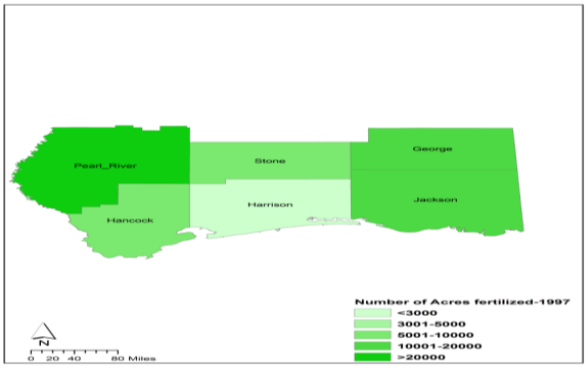

Fig. 10 Number of Acres Fertilized 1997

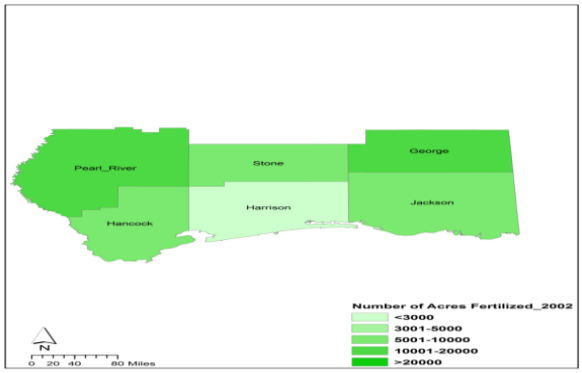

Fig. 11 Number of Acres Fertilized 2002

The spatial aspects of the indicators threatening streams such as the number of acres covered with fertilizer during the periods of 1992, 1997 and 2002 are represented in Fig. 9, 11 and 12 under four classes. In Fig. 9 to 12 the significant classes of >20000 acres to 10001 - 20000 represent the high number of acres treated with fertilizer. The medium class refers to the 5000 to 10000 acre types while the lower types consist of those classified as 3001-5000 coupled with the < 3000 category.

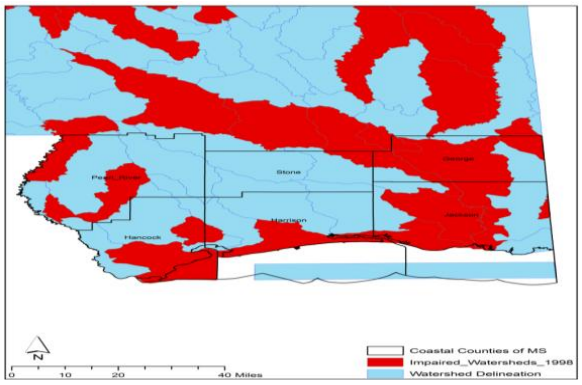

Fig. 12. Impaired Watersheds Due to Nutrient Flow 1998

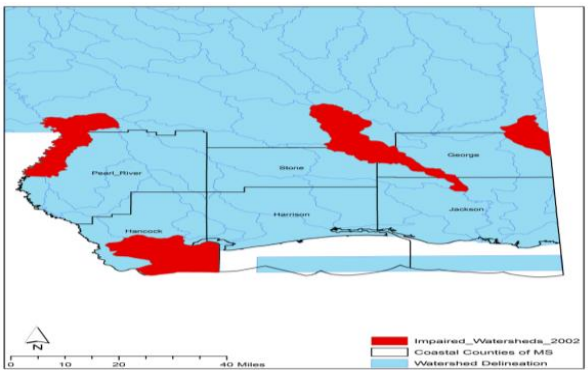

Fig. 13. Impaired Watersheds Due to Nutrient Flow 2002

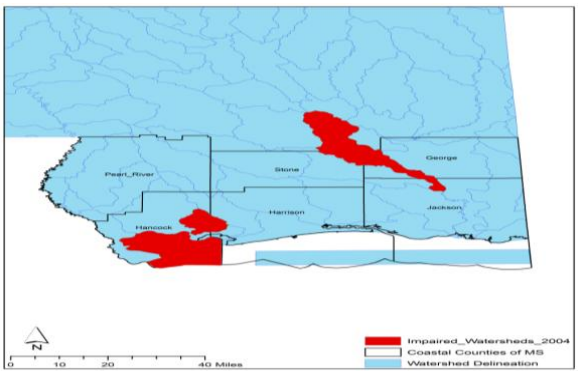

Fig. 14 Impaired Watersheds Due to Nutrient Flow 2004

The number of acres under fertilizer use across space as the map shows seemed quite pronounced in the periods of 1992, 1997 and 2002 in some counties. Note that the Northern portion of the study area map highlighting Pearl River County had fertilized areas exceeding 20000 acres. Fertilizer use not only reached high levels, but the Northern part appeared as the area with more fertilized areas in the 1992, 1997, and 2002 fiscal years (Fig. 9, 10, 11). The information on fig. 12 to 14 describe impaired watersheds, coastal counties and the watershed delineation. Impaired watersheds as shown in the figures stand for degraded watersheds, coastal counties are those geographic units located around the coast line while watershed delineation deals with demarcation around it. Turning to impaired watersheds from nutrient flow in the coastal counties, there was a high concentration of impaired water areas in the 1992 period with much of it located at George and Jackson, Harrison, Hancock and Pearl River. A closer look on the maps during the year 2002 and 2004 indicates a slight recurrence of impairment in minute clusters within the three counties most notably Hancock, George and Jackson (Fig. 12-14).

VI. Discussions

The snapshot of the discharge and transfer of various pollutants as wells as fertilizer application and the case of impaired waters and the presence of environmental stressors in the region show they pose serious threats to the surrounding ecology of the area. Regarding the environmental analysis, it is evident from the tables that the total amount of environmental contaminants in the study area reached sizable levels over the years (Tables 2-7). A case in point is the Pearl River county area where the quantity of air pollutants discharged into the atmosphere by industries stood at 1,903,364 pounds within the 12 year period of 1988 and 2000. Among the other indicators, the volume of total environmental releases, offsite transfers and total production of related wastes amounted to 1,125373, 634,464 and 4,561,438 pounds during the same periods (Table 2).

Another point worthy of note is that Stone County's total offsite transfers of pollutants which reached significant levels were in the order of 30,625, 32,384, and 34,793 in 2000, 2001 and 2002 respectively. All in all in the years under analysis, the six major counties of the region experienced high, medium and low levels of pollution large enough to severely alter the carrying capacity of an ecosystem already stretched beyond limits (Table 4). Even though in the various category of pollution indicators, smaller counties produced volumes of pollutants proportional to the number of sources in those areas. The three other counties of Jackson, Harrison, and Hancock accounted for the highest volumes of total environmental toxins that were released in the region. The quantity of these pollutants measured in tens, hundreds of thousands and hundreds of millions of pounds in wastes are lethal enough to degrade the environment (Table 5-7).

Of great concern in terms of policy and abatement is the degree to which large environmental releases

from air, water, and land contaminants, underground injection of chemicals, off site transfer of pollutant and industrial production of wastes remain fully concentrated in the region (Table 2-5). Regarding the temporal distribution of fertilizer or agrochemicals, the application levels grew extensively in double digits at Harrison, Hancock, George, and by triple digits in Jackson. On the acreages of land treated with fertilizer, the counties of Pearl River and George appear to have exceeded the other areas in the use of fertilizer nutrients. The applications of fertilizers in Pearl River ranged from about 32,262 acres in 1992, 28,907 during 1997 and 14,234 by 2002. Over the years (1992, 1997, and 2004) at George County, the area of agricultural land covered with fertilizer was estimated at 16,484, 11,907 and 19,395 acres respectively (Table 8).

On the percentages of change, see that the counties were evenly split in terms of declines and gains in 1992 -1997. In fact, three counties (Harrison, Hancock and Jackson) made gains while three other areas most notably Pearl River, George and Stone and others saw their acreages of fertilized land decline. In the fiscal year of 1998, impaired water areas seemed more frequent in South Mississippi urban areas. In that period, other counties most notably Pearl River, Harrison, and Hancock experienced impairment in 2 major water areas. The same can be said of 2002 and 2004 when George and Hancock each had similar numbers in impaired water areas (Table 8). On pollution sources among the counties, see that the petrochemical, power and utility industries operating in the area emerged as some of the largest contributors (Table 9). A simple correlation analysis performed on selected variables shows a positive relation between impaired waters and fertilized acres of farmland to show interconnectedness.

The study area also experienced the effects of several other miscellaneous pollutants that are hazardous to the region's environment (see Appendix). The potential impacts mostly impairment of watersheds, rising number of impaired water bodies, the flow of fertilizer run off and nutrients into sensitive stream habitats of the area raises the risks of ecosystem degradation and pollution. The perverse nature of the problem not only threatens the different life forms in the environment but it diminishes ecosystem quality and livability of cities in the large metro areas of Southern Mississippi coastal environments.

A temporal spatial analysis using GIS to map the widespread discharge of chemical contaminants revealed a gradual spreading of pollutants, elevated risks to the sensitive coastal ecosystem and exposure to cancer risks for residents of the area. There exists also enormous geographic diffusion of animal wastes in some of the counties where quite a number of houses have come under high risk exposures to lead hazards. In the context of the region, GIS provides decision makers the capability for locating and appraising the quantity of pollutants and their impacts.

Public policy will benefit more from the adoption of remedies geared at improving environmental quality through the enforcement of standards and the use of efficient abatement techniques to contain pollution. Some of the remedies should include strengthening existing policies, disclosure of emission sources, funding assistance, the design of emission information system and data infrastructure.

The thing to draw from the tabular analysis is that the pollution trends herein identified and the widespread use of fertilizers and the threats faced by the watersheds in the region do not operate in a vacuum. The emerging stressors and pollutants known to impact the environment are driven by industrial activities, agricultural farming and human presence. The fact that the sources of these pollutants are induced by human factors does re-echo the human nature interface debate that has lingered on in theoretical circles over the years. Highlighting the extent of this interface, in the context of the study area of Southern Mississippi region and the pollution threats, stands as a major contribution to the literature.

Theoretical Importance

The paper reaffirms the theory of human interactions with nature. Humans depend on nature for several things ranging from survival to the livability of communities. Currently, there seems to be a growing concern about the impact of economic activities on the environment and the rate at which industrial activities overstretch the capacity of natural systems to provide services as shown in Southern Mississippi. The sequential mapping and appraisal of the emerging stressors and their locations using GIS can serve as effective decision support tool for managers and communities in Southern Mississippi craving for a livable environment. With the growing stress inflicted on ecosystems, ecological consciousness has created a need for analyzing the interfaces existing among the various segments of the economy and the environment spatially.

In this setting, comprehensive pollution analysis for ecosystem protection is regarded by most managers

as a necessary complement to effective environmental decision. Whether the goal is pollution prevention or some broader notion of sustainability, there is a widespread belief that sequential mapping of the stressors will help polluters identify and implement desirable environmental innovations. Moreover, environmental regulation is evolving toward public policies that rely mostly on the collection and reporting of environmental information anchored in pollution analysis and mapping of the stressors based on an understanding of nature –human interface debate.

There are also several important theoretical observations that have emerged in this study. Since the gradual acceptance of GIS as visualization tool for mapping the impacts of human nature interface in the public environmental health arena, pollution analysis as presented in this paper has continued to play a vital role by encouraging the adoption of theoretical tools for strengthening policy making. Given its current importance, human nature interaction theory, as conceptualized in the project, provides planning and policy the abundance of learning tools for enriching the intellectual and philosophical orientation of those attuned to theory and practice. This can go a long way in making the professionals promote the role of theories of human nature interaction as a road map to strengthening policies pertaining to pollution prevention. This theoretical revival brought about by GIS applications as a vital tool stems partly from the global call to action towards the adoption of spatial technologies in analyzing the impacts of human nature interaction in fragile environments.

In that regard, the ideas shaping GIS applications in pollution trends, as presented in the paper helps stimulate the interest and opportunities that are currently driving the course of research in environmental change. Additionally, the theoretical underpinnings of human-environment interaction have also widened the methodological options for planning. They are essential in addressing the ecological problems central to good decision making and for improving the treatment of nature during industrial activities. The familiarity with devices such as GIS in showing spatial patterns of various stressors associated with pollution continues to show promise. It remains germane in tracking the externalities from industrial activities spatially and their impacts on the natural environment. This can set the stage for continuous use of these approaches in future studies. The models used here can also be instrumental in encouraging the adoption of spatial technologies in identifying patterns of ecosystem disturbance and mitigation measures. They are relevant for planning in coastal environments such as the South Mississippi region. The methodology of this project can be used to sustain future research in the mapping of stressed environments and the ongoing human-nature interface debate.

The Benefits of GIS Methodology

The GIS mapping highlighted the spatial distribution of pollution indicators and the close proximity between sites of pollution and a fragile costal environment of the state as well. In the current study, the availability of temporal spatial data and analysis played a vital role in facilitating the assessments of the ecological risks emanating from industrial activities. The assemblage of the information and analysis using the mix scale methodology as an emerging science devoted to the study area, not only quickened the data processing stage of the study, but it unveiled the location of stressors in the South Mississippi region. It is essential for effective management and timely mitigation.

Accordingly, GIS analysis in this paper as a contribution the literature, stands as a relevant decision support tool for pinpointing high risk areas and watersheds threatened by environmental externalities. In the study area, this involved the generation of maps that identified externalities such as animal wastes, TRI sites, lead hazards, cancer risks, and surface water impairment. Visualizing metro areas and natural features prone to ecological stress in these settings, not only helped focus the scope of GIS and environmental planning with records of change in affected areas, but it furnished information on the pace at which industrial activities impact nature.

For the purposes of planning, spatial analysis offered a visual documentation of the state of the environment at precise locations on different sets of variables related to industrial activities in Southern Mississippi. With the capability to generate temporal spatial information, this perspective serves the needs of decision makers in weighing the significance of the emerging patterns and the impacts on the local ecosystem. Without access to such information, planners run the risk of offering improper blue prints and solutions for protecting the environment. GIS applications, can be effective as part of an emerging science for addressing these concerns by providing managers a yardstick for analyzing different levels of changes in the ecosystem. It is expected that they will serve a useful purpose in subsequent research and will

evolve further through utilization in a variety of situational settings in the study area and elsewhere under conditions that are compatible with the ideas of environmental planning.

The study also serves as a conduit for future applications in the coastal areas of states or regions. This then stimulates the growth of regional expertise and confidence which in turn enhances the capacity to make decisions in areas associated with industrial activities and ecosystem impacts. This role of GIS as decision support tool, can lead to a real consensus as more users, and those in charge of policy making have faith in the approaches and make a conscious decision to increase their application in future. The applications of this technique in the research along with the findings from it therefore make a contribution to our understanding of GIS applications in the mitigation of pollution and environmental analysis. These techniques play a fundamental role with the steps upon which impact analysis of pollution activities is built. The project has revealed the utility of GIS applications in environmental planning and pollution mitigation and thus serves as conduit for future applications as an emerging science in communities impacted by pollution activities.

VII. Conclusion

Temporal-spatial tracking of pollution sources in the region point to heavy involvement of industrial activities in the petrochemical sector, power, utilities,agriculture and others. The perverse nature of the problem not only threatens the different life forms in the environment, but it diminishes ecosystem quality and the livability of cities.

Using geospatial technology of GIS, the paper shows that human-environment interaction involving pollution intensive industries in the Gulf Coast region fuels the concentration of several chemical elements lethal enough to inhibit sensitive estuarine ecosystem of the area. Compounding the matter is the impact of current practice of underground injections of pollutants, off site transfers, production related waste and fertilizer use in the areas. Ecological stressors made up of fertilizer applications, number of impaired watersheds, and pollution inventory sites were on the rise especially in areas adjacent to stream corridors. The pressures unleashed from these pollution variables as the analysis shows puts enormous strain on the region's air and water quality. All these raised the level of stress on the region's environments.

The GIS mappings highlighted the spreading of housing units exposed to the risks of lead hazards and the severity of pollution. The mappings also indicated the geographic diffusion of cancer risks from several stressors such as hazardous air pollutants, chemical releases and surface water with reported pollution problems along the watersheds. Other aspects of the GIS analysis highlighted the spatial diffusion of toxic release inventory sites and the location of animal waste release. The mapping of pollution predictors in environmental planning in those settings can assist in determining critical areas. This can enhance the monitoring and the introduction of pollution abatement programs in affected counties along the Southern Mississippi region. The study also highlighted the theoretical essence of the research and the importance of GIS. As part of the remedies, the paper offered six recommendations: strengthening existing policy, disclosure of emission sources, funding assistance; design of geo emission information system and the development of adequate data infrastructure, requiring government enforcement of air quality standards and the design of new methods for reaching them.

Finally, the expectation is that familiarity with devices such as Geographic Information Systems remains pertinent in showing spatial patterns of various stressors associated with pollution. They are vital tools for locating industrial activities fuelling recurrent externalities and their impacts on the natural environment. This can set the stage for continuous use of these approaches in future studies and education. The models used here can also be instrumental in encouraging the adoption of geospatial information technologies in identifying patterns of ecosystem disturbance and mitigation measures. They are relevant for resource planning in coastal environments such as the South Mississippi region.

REFERENCES

[1] Arnoff. S, "Geographical Information Systems: A Management Perspective," WDL Publications, Ottawa, (1989).

[2] Burnett. R, Ma. R, Jerrett. M, Goldberg. M.S, Cakmak.S, Pope 3rd. C.A and Krewski. D, "The spatial association between community air pollution and mortality: a new method of analyzing correlated geographic cohort data," Environmental Health Perspectives, Vol.109, 2001, pp. 375–380.

[3] Buzzelli. M, Jerrett. M, Burnett. R and Finklestein. N, "Spatiotemporal perspectives on air pollution and environmental justice in Hamilton, Canada, 1985–1996," Annals of the Association of American Geographers, Vol.93, 2003, pp 557–573.

[4] DeMers. M.N, "Fundamentals of Geographic Information Systems," Wiley, New York, (1997).
[5] Dennison William. C, "Environmental problem solving in coastal ecosystems: A paradigm shift to sustainability," Estuarine, Coastal and shelf science, 2007, pp 3-4.
[6] Doern.Bruce and Seymour.Wilson, "Issues in Canadian Public Policy," Macmillan , Ottawa, (1974).
[7] Estes. Larry, "Basin Profile: Pascagoula River Basin," Environmental News, Vol.3, 2006, pp 4-5.
[8] Gatrell. A.C and Loytonen. M, "GIS and Health Research: An Introduction," GIS and Health, Taylor & Francis, London, 1998, pp 3–16.
[9] Jerrett. M, "A GIS-environmental justice analysis of particulate air pollution in Hamilton Canada, " Environment and Planning A, Vol.33, 2001, pp 955–973.
[10] Miller.J.R, " The control of mosquito-borne diseases in New York City," Journal of Urban Health,Vol.78, 2001, pp 359–366.
[11] Mississippi Department of Environmental Quality (MDEQ), "Pascagoula River Basin". Available from: http://www.deq.state.ms.us/mdeq.nsf/page WMB_ Pascagoula_ River_ Basin? [Accessed on 3/10/2007], 2007.
[12] Mossa.Joan,and Coley. David, "Platform Changes In Rivers With and Without in stream and Floodplain Sand and Gravel Mining: Assessing Instability In The Pascagoula River Tributaries, Mississippi," Department of Geography, University of Florida, Gainesville, (2005).
[13] Natural Resources Conservation Services (NRCS), "Pascagoula River Watershed". Available from http://www.ms.nrcs.gov/programs /Pascagoula, [Accessed on 3/10/2007], 2007.
[14] Pikhart. H, Prikazsky. V, Bobak. M, Kriz. B, Celko.M, Danova. J, Pyrl and K, Pretel. J, "Association between ambient air concentrations of nitrogen dioxide and respiratory symptoms in children in Prague, Czech Republic.Preliminatry results from the Czech part of the SAVIAH study. Small area variation in air pollution and health," Central European Journal of Public Health, Vol.5, 1991, pp 82–85.
[15] Pikhart. H, Bobak. M, Gorynski. P, Wojtyniak. B, Danova.J, Celko. M.A, Kriz. B, Briggs and D, Elliott. P, "Outdoor sulphur dioxide and respiratory symptoms in Czech and Polish school children: a small-area study (SAVIAH). Small- Area Variation in Air Pollution and Health," International Archives of Occupational Environmental Health , Vol.74, 2001, pp 574–578.
[16] Schwetz. B, Mast. T, Weigerl. R, Dill and T, Morrisey. R, "Developmental toxicity of inhaled methyl ethyl ketone in mice," Fundamental and applied toxicology,Vol.16, 1991, pp 742-748.

Table 1. The Study Area of Southern Mississippi Region

County	Population	Area in Square Miles	CMA
Pearl River	57,099	811	Picayune
George	21,828	478	Pascagoula,
Stone	15,608	445	Gulfport-Biloxi,
Harrison	171,875	580	Gulfport-Biloxi,
Hancock	40,421	476	Gulfport-Biloxi
Jackson	130,577	726	Pascagoula
Total	437408	3516	NA

Source: US Census Bureau

Table 2. Environmental Releases For Pearl-River County

Year	Air releases	Water releases	Land releases	Underground injection	Total Environmental releases	Total Off-site transfers	Total production-related waste
1988	8,864	12,850	0	0	21,714	2,208	NA
1989	41,351	5,600	0	0	46,951	13	NA
1990	243,016	1,100	0	0	244,116	43	NA
1991	229,101	0	0	0	229,101	467,050	1,093,397
1992	129,386	0	0	0	129,386	1,860	415,853
1993	99,312	500	0	0	99,812	3,865	326,423
1994	65,428	430	0	0	65,858	7,207	409,273
1995	65,923	0	0	0	65,923	10,607	337,878
1996	60,724	12	0	0	60,736	5,207	321,317
1997	47,845	0	0	0	47,845	108,338	268,801
1998	40,921	0	0	0	40,921	9,248	336,564
1999	22,965	0	0	0	22,965	6,337	248,065
2000	17,991	0	0	0	17,991	2,399	213,027
2001	18,225	0	0	0	18,225	2,748	293,663
2002	99312	500	0	0	99812	7334	297177
Total	1190364	20992	0	0	1211356	634464	4561438

Source:www.scorecard.org

Table 3. Environmental Releases For George County

Year	Air releases	Water releases	Land releases	Underground injection	Total Environmental releases	Total Off-site transfers	Total production-related waste

1988	250	0	0	0	250	750	NA
1989	750	0	0	0	750	0	NA
1990	765	0	0	0	765	44,499	NA
1991	0	0	0	0	0	8,501	426
1992	0	0	0	0	0	13,000	426
1993	0	0	0	0	0	22,500	8,300
1994	0	0	0	0	0	11,751	100
1995	0	0	0	0	0	0	0
1996	0	0	0	0	0	0	0
1997	0	0	0	0	0	5,250	0
1998	0	0	0	0	0	0	0
1999	0	0	0	0	0	2,175	0
2002	18195	0	1500	0	19695	2750	19695
Total	19960	0	1500	0	21460	111176	28947

Source: www.scorecard.org

Table 4. Environmental Releases For Stone County

Year	Air releases	Water releases	Land releases	Underground injection	Total Environmental releases	Total Off-site transfers	Total production-related waste
1988	290	0	0	0	290	6	NA
1989	583	0	0	0	583	4,507	NA
1990	36,033	0	0	0	36,033	5,455	NA
1991	35,043	0	0	0	35,043	1,013	38,896
1992	25,036	0	0	0	25,036	708	28,406
1993	18,026	651	0	0	18,677	213	21,887
1994	16,023	256	0	0	16,279	75	18,492
1995	8	49	0	0	57	104	3,706
1996	4,218	24	0	0	4,242	778	13,337
1997	3,118	43	0	0	3,161	2,712	7,975
1998	8,519	25	0	0	8,544	4,765	16,066
1999	11,919	61	0	0	11,980	6,397	22,307
2000	13,014	52	0	0	13,066	30,625	43,677
2001	14,463	230	17	0	14,710	32,384	78,195
2002	7193	260	79	0	7532	34793	43012
Total	193486	1651	96	0	195233	124535	335956

Source: www.scorecard.org

Table 5. Environmental Releases For Harrison County

Year	Air releases	Water releases	Land releases	Underground injection	Total Environmental releases	Total Off-site transfers	Total production-related waste
1988	6,937,589	13,463	2,200,000	40,500,000	49,651,052	28,942	NA
1989	6,167,790	11,660	0	37,000,000	43,179,450	46,052	NA
1990	6,091,461	11,766	2,015	33,000,000	39,105,242	31,867	NA
1991	6,335,430	3,985	520	41,000,000	47,339,935	137,909	51,752,479
1992	4,200,325	6,435	2,670	52,000,000	56,209,430	296,664	63,522,706
1993	3,154,506	10,700	2,314	56,000,000	59,167,520	544,148	67,439,661
1994	3,313,910	7,850	2,410	57,000,000	60,324,170	1,136,491	67,566,902
1995	2,307,300	5,162	0	0	2,312,462	994,206	8,479,587
1996	2,191,060	535	4	0	2,191,599	801,371	9,760,053
1997	2,165,067	15	0	8,448,000	10,613,082	1,215,912	19,134,816
1998	8,471,453	4,575	666,934	6,880,000	16,022,962	308,598	25,738,073
1999	11,034,704	4,060	770,612	8,235,100	20,044,476	247,959	27,984,699
2000	12,384,227	6,020	1,015,125	12,557,081	25,962,453	248,485	34,816,983
2001	5,669,347	12,710	1,432,377	11,035,253	18,149,687	264,979	29,039,834
2002	4337670	1124	1505911	11614190	17469015	76186	26279003
Total	84761839	100060	7600892	375269624	467742535	6379769	431514796

Source:www.scorecard.org

Table 6. Environmental Releases For Hancock county

Year	Air releases	Water releases	Land releases	Underground injection	Total Environmental releases	Total Off-site transfers	Total production-related waste
1988	705,054	1,500	1,000	0	707,554	286,936	NA
1989	544,525	1,080	3,750	0	549,355	746,498	NA
1990	222,262	83	2,265	0	224,610	646,542	NA
1991	19,412	35	1,770	0	21,217	370,064	1,322,162
1992	16,718	0	0	0	16,718	254,963	1,021,113
1993	14,060	5	0	0	14,065	180,172	619,796
1994	22,194	5	0	0	22,199	345,947	1,003,482
1995	20,500	5	0	0	20,505	640,760	1,142,650
1996	48,517	255	0	0	48,772	460,685	999,467
1997	11,600	0	0	0	11,600	1,386,500	1,172,010
1998	79,668	20	0	0	79,688	506,205	1,189,576
1999	86,495	30	0	0	86,525	601,730	48,447,102
2000	84,148	35	0	0	84,183	586,587	75,321,377
2001	101,189	320	0	0	101,509	767,805	75,424,892
2002	52222	857	0	0	53079	1082723	76209833
Total	2028564	4239	8785	0	2041579	8864117	283873460

Source: www.scorecard.org

Table 7. Environmental Releases For Jackson County

Year	Air releases	Water releases	Land releases	Underground injection	Total Environmental releases	Total Off-site transfers	Total production-related waste
1988	4,271,088	248,275	153,464	3,000	4,675,827	4,744,023	NA
1989	3,072,412	868,931	5,881	3,000	3,950,224	488,331	NA
1990	3,561,912	656,375	17,331	1,000	4,236,618	315,389	NA
1991	4,551,134	903,012	10,172	1,807	5,466,125	4,078,875	80,494,344
1992	3,971,706	479,536	131,201	2,737	4,585,180	3,017,425	128,962,604
1993	3,762,441	367,659	132,217	52,872	4,315,189	192,706,729	313,088,888
1994	3,021,242	43,777	133,198	32,511	3,230,728	2,385,115	152,541,845
1995	3,808,062	85,200	151,898	82,251	4,127,411	2,041,550	156,270,179
1996	4,921,966	271,061	167,521	83,315	5,443,863	2,355,768	151,772,674
1997	3,904,709	360,494	281,477	96,641	4,643,321	5,891,740	166,186,058
1998	3,278,623	455,566	1,111,764	12,506	4,858,459	5,635,490	204,362,692
1999	3,577,822	191,648	432,834	91,662	4,293,966	10,013,832	39,959,773
2000	4,521,319	144,478	1,693,640	34,637	6,394,074	10,984,308	38,766,701
2001	5,312,888	87,997	868,430	11,648	6,280,962	7,478,798	38,722,031
2002	3916645	170617	478485	0	4565746	5321329	29549295
Total	59453969	5334626	5769513	509587	71067693	257458702	1500677084

Source: www.scorecard.org

Table 8. The Distribution of Fertilizer Use and Impaired Waters In Southern Mississippi Counties

Acres Fertilized					
Counties	1992	1997	2002	% Change(1992-1997)	% Change(1992-2002)
Pearl River	32262	28,907	14,234	-10.39	-50.75
George	16,484	11,907	19,395	-27.76	62.88
Stone	8846	8,671	8,886	-1.978	2.47
Harrison	3530	4,514	4,323	27.87	-4.23
Hancock	6135	9,271	7,062	51.11	-23.82
Jackson	3511	11,882	8,779	238.42	-26.11
Impaired Water areas					
Counties	1998	2002	2004	% Change(1998-2002)	% Change(2002-2004)
Pearl River	2	1	0	-50	-100
George	5	2	1	-60	-50
Stone	1	1	1	0	0
Harrison	2	0	0	-100	
Hancock	2	1	2	-50	100
Jackson	5	1	1	-80	0

Source: www.scorecard.org

Table 9. Pollution Sources in the southern Mississippi Counties

Source Pollutant	Location	Pounds of chemicals released	% contributed to the total release
Valspar Refinish InC.	Picayune (Pearl River County)	10021	72.46
Pearl River wood L.L.C.	Picayune (Pearl River County)	2939	21.25
Arizona Chemical Co. Picayune	Picayune (Pearl River County)	869	6.28
American Tank & Vessel Inc.	Lucedale (George County)	18195	92.38
Tri-State Pole & PIling Inc.	Lucedale (George County)	1500	7.616
Desoto Treated Materials Inc.	Wiggins (Stone County)	7277	96.61
International Paper Co.	Wiggins (Stone County)	135	1.79
Hood Inds. Inc.	Wiggins (Stone County)	120	1.59
Dupont Delisle Plant	Pass Christian (Harrison County)	14894376	85.26
Mississippi Power Co. Plant Watson	Gulfport (Harrison County)	2329539	13.33
Hartson-Kennedy Cabinet Top Co. Inc.	Gulfport (Harrison County)	200490	1.147
Ershigs Biloxi	Biloxi (Harrison County)	21172	0.12
LightHouse Marble	Biloxi (Harrison County)	20680	0.11
Taber Metals Gulfport L.P.	Gulfport (Harrison County)	1654	0.01
Northrop Grumman Ship Sys. Inc. - Gulfport Ops.	Gulfport (Harrison County)	1104	0.01
Wellman OF Mississippi Inc.	Bay Saint Louis (Hancock County)	27508	51.82
GE Plastics	Bay Saint Louis (Hancock County)	14985	28.23
NASA John C. Stennis Space Center	Stennis Space Center (Hancock County)	10011	18.86
Polychemie (Port Bienville Plant)	Pearlington (Hancock County)	575	1.083
Mississippi Power Co. Plant Daniel	Escatawpa (Jackson County)	1783848	39.07
Chevron Prods. Co. Pascagoula Refy.	Pascagoula (Jackson County)	1254077	27.46
Mississippi Phosphates Corp.	Pascagoula (Jackson County)	1137379	24.91
Northrop Grumman Ship Sys	Pascagoula (Jackson County)	306243	6.7
First ChemicaL Corp.	Pascagoula (Jackson County)	34792	0.76
Omega Protein Inc.	Moss Point (Jackson County)	23129	0.5
Ferson Optics Inc.	Ocean Springs (Jackson County)	13680	0.29
Shipley Co. - Moss Point P lant	Moss Point (Jackson County)	8932	0.19
Rolls-Royce Naval Marine Inc.	Pascagoula (Jackson County)	2222	0.048
Automatic Processing Inc.	Moss Point (Jackson County)	1445	0.03

Source: www.scorecard.org

APPENDIX I

Table: Miscellaneous Environmental indicators (*per 1,000,000)

County	Levels of Pollution	Percentage changes in TRI releases	Percentage of housing nits with lead hazards	Number of TRI sites releasing chemicals	*Cancer risks from Hazardous air pollutants	Percent of surface waters with reported problems	Percent change in release of Animal waste
Pearl_River	20%	-31%	2%	3	300	86%	-21%
George	30%	77.78%	2%	1	240	63%	-4%
Stone	20%	24.97%	2%	3	260	95%	17%
Harrison	100%	-65%	1%	6	370	100%	21%
Jackson	100%	-1%	1%	10	500	79%	-20%
Hancock	70%	-92%	2%	3	320	85%	13%

A Joint Scheduling and Mapping Method for Dynamically Reconfigurable SoCs Interconnected by an on-chip Mesh Network

Ling Wang[a], Xiangnan Sui[a], Yingtao Jiang[b]

[a] School of Computer science and technology, Harbin Institute of Technology, Harbin China
[b] Department of Computer and Electrical Engineering, University of Nevada, Las Vegas, USA

Abstract—Reconfigurable SoC interconnected by an NoC architecture mandates a low power and small footprint reconfiguration scheme that enables multiple applications to effectively share precious hardware resources. The trade-offs between the static compilation and the dynamic reconfiguration has yet to be evaluated at the highest possible abstraction level of the NoC designs. In this paper, reconfiguration is thus considered during the application scheduling and mapping stage. That is, for a given set of applications which target to run on a dynamically reconfigurable NoC architecture, a schedule and map of these applications needs to be found to minimize the communication cost, while satisfying the timing, area and other applicable design constraints. The proposed solution follows a three-step design flow. In the first task scheduling step, multiple applications are scheduled to a minimal number of processor nodes while meeting the timing constraints. Next, applications that shall be mapped onto the same hardware resource but run at the different time instances through hardware reconfiguration are merged. In this step, effort is dedicated to minimize the reconfiguration cost. In the last step, all the applications are finally mapped onto the targeted NoC architecture. The experiment results have shown that the proposed method has achieved 50% area reduction than a conventional scheme that does not consider reconfiguration cost.

Keywords—NoC, Mapping, scheduling, reconfiguretion

I. Introduction

SoC (Systems on Chip) designs have shown rapid growth in complexity with an increasing number of integrated processors, memory, accelerators, and various other types of IP cores [5][20]. Networks on chip (NoC), due to their structural advantages and modularity [2], have emerged as the design paradigm for connecting the many on-chip cores in SoCs. The choice of network topology as well as mapping and routing strategies adopted has direct implications on the network merits, such as the average inter-IP distance, the total wire length, and the communication load distributions, which in turn, determine the power consumption and the average latency of the network. The topologies proposed for on-chip networks vary significantly from regular, tiled-based architectures [5][6] to fully customized ones [7][10][11]. Since a fully customized NoC is designed and optimized for a specific application, it gives the best performance and power results just for that application. On the other hand, reconfigurable NoCs, where network topology, routing protocols and even some of the IP cores can be altered, can deliver the optimal performance and power result across all the target applications. Through reconfiguration, hardware resources can be optimized for each application that often has different functionalities and communication characteristics from the other applications. Yet in this case, the trade-offs between the static compilation and the dynamic reconfiguration have to be carefully evaluated at the highest possible abstraction level of the NoC designs, particularly at the application scheduling and mapping level.

There have been several studies that attempt to deal with mapping of the multiple applications onto reconfigurable NoC architectures [8, 9]. In [8], a worst-case-based mapping method was proposed, where the cores and the NoC are mapped to satisfy the most serious constraints imposed by all the target applications. In [9], a method that maps multiple applications based on the traffic characteristics of a single application was proposed. After application mapping, a reconfigurable NoC is created by embedding programmable switches between any two routers of a mesh-based NoC, but these programmable switches unfortunately have very high area penalty which can impose a serious problem to NoC designs. Even more noticeable, neither of the two schemes [8, 9]

Corresponding Author: Ling Wang, Email Address: wangling@hit.edu.cn

has considered reconfiguration cost during the mapping and route determination process.

One big drawback of these approaches is that they all target to find a suitable mapping solution without considering the cost associated with dynamic reconfiguration. In [18], a mapping flow is proposed for dynamic reconfigurable platform where reconfiguration cost is indeed minimized along with communication cost. However, scheduling, which preferably shall be considered along with the mapping, is actually absent from the proposed flow.

To address the above problems, a scheduling and mapping scheme is proposed, and this new scheme attempts to balance both the reconfiguration cost and the communication link cost. That is, in the core mapping phase, rather than mapping tasks directly onto the physical NoC, tasks are first mapped to virtual cores, which are then mapped onto the physical NoC. The proposed scheme thus is divided three major steps which include scheduling, core mapping, and eventually NoC architecture generation.

In this paper, to overcome the aforementioned problems, an integrated scheduling and mapping scheme is proposed. In specific, when scheduling is performed, each task of the target applications will be first scheduled to virtual cores, after which these virtual cores will be mapped to the physical cores of a NoC. Note that reconfiguration cost is considered along this scheduling and mapping process, and thus the communication cost will be eventually minimized.

The rest of the paper is organized as follows. In Section 2, a general dynamically reconfigurable NoC architecture is briefly introduced. The design flow and a motivation example are presented in Section 3. The three phases of the proposed design scheme are detailed in Section 4. Experiment results are reported in Section 5, and conclusions are finally drawn in Section 6.

II. Dynamically Reconfigurable NoCs

In a reconfigurable, mesh-based interconnection network that is of a concern to this paper, a router is connected directly to its adjacent routers and all the routers are connected to a reconfiguration controller, as shown in Fig. 1 [16]. Here the Reconfiguration Controller (RC) is tasked to control the reconfiguration process, and its basic components include the Repository, the Configuration Port (CP) and the Reconfigurable Interface (RI). The Repository contains a memory unit that stores the reconfigurable modules' configuration data, bearing a great similarity to the configuration files used for configuring an FPGA chip. The RI is necessary to implement a static routing between a reconfigurable module and the rest of the system. All the reconfiguration-related activities, including changes of network topology, routing protocols and/or IP cores, are controlled by this reconfiguration controller. In general, dynamic hardware reconfiguration can only be implemented on dynamically reconfigurable devices. Thus, FPGAs are used in this study.

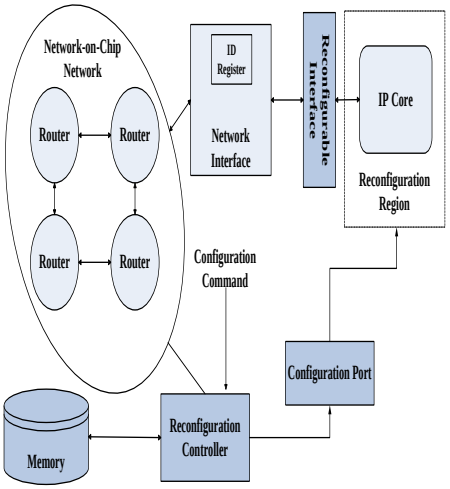

Fig. 1. The Reconfigurable NoC model

III. Problem Formulations

Definition 1: A task graph TG (V, E) is an acyclic directed graph that represents an application, with each vertex $v_i \in V$, representing a task, and an edge between two vertices v_i and v_j, denoted as $e(v_i, v_j) \in E$, representing a communication link between v_i and v_j. The weight of edge $e(v_i, v_j)$ represents the communication bandwidth required between v_i and v_j.

Definition 2**:** A core graph VP (U, L) is an undirected graph, with each vertex $u_i \in U$ representing a virtual core node, and the edge between two vertices u_i and u_j, denoted as $l(u_i, u_j) \in L$, representing a communication link between u_i and u_j. The weight of edge $l(u_i, u_j)$ represents the communication bandwidth between u_i and u_j.

Definition 3: An NoC topology architecture graph AG (Q, R) is an undirected graph, with each vertex $q_i \in Q$ representing a core node in the NoC topology and the edge between two vertices q_i and q_j, denoted as $r(q_i, q_j) \in R$, representing a communication link between q_i and q_j. The weight of edge $r(q_i, q_j)$

represents the communication bandwidth between q_i and q_j.

The problem that attempts to schedule and map multiple applications onto an Network-on-Chip architecture is defined as follows:

Given a set of applications, applications 1, 2, …i,…, A, represented by a set of task graphs, TG = { TG_i (T_i, R_i), i=1， …, $|A|$}, and a number of IP cores, find a mesh architecture AG that connects all the IPs, and schedule and map these applications onto these IP cores with minimum communication cost,

$$totalcom = \sum_{j=1}^{|E|} B(e_j) dist(source(e_j, dest(e_j))$$

while satisfying the area and timing constraints. Here

(i) area is determined as the number of mapped nodes on the AG;

(ii) timing is defined as the scheduling time of the TG;

(iii) e_j is the flow in the input task graphs TG and $|E|$ is the total number of flows of TG;

(iv) $B(e_j)$ is the bandwidth of the flow e_j in the topology architecture described as AG;

(v) Source(e_j) and dest(e_j) represent the source and the destination nodes of flow e_j in the TG, respectively;

(vi) dist(source(e_j), dest(e_j)) represents the hop count between source(e_j) and dest(e_j) with pre-determined routes in AG, assuming XY routing is adopted.

The above problem is a special case of processor scheduling that is known as NP-complete. Thus, a heuristic algorithm is developed to solve the above problem. In the literature, various topologies [2], including Mesh, torus, GNLS [16] and etc., have been proposed for NoC designs. In this paper, although we concentrate on the mesh topology, the proposed method can be readily applied to other topologies.

IV. Design Flow of Scheduling and Mapping Applications onto Reconfigurable NoCs

An example is given to illustrate how system performance is impacted when reconfiguration is considered during the scheduling and mapping stage. Two parallel applications a1 and a2 are shown in Fig.2.a and 2.b, respectively, and their respective core graphs generated after scheduling are shown in Fig.2.c and 2.d.

If reconfiguration cost is not considered during scheduling/mapping, these two core graphs (Fig. 2.c and 2.d) are mapped to the topology one at a time. As a result, the total communication cost is 140 and the area cost is 5 (Fig. 2.g). But if reconfiguration cost is considered after scheduling, one can see that as V2 and V3 run at different time slots, they actually can be reconfigured and mapped to the same core as shown in Fig. 2.e. As such, the area cost now drops to 4, and its total communication cost is 132, as shown in Fig. 2.h. Further reduction of the reconfiguration cost is possible. Instead of having V2 and V3 run on the same core through reconfiguration, if V2 and V4 are actually mapped to the same core, as shown in Fig. 2.f, the area cost after scheduling and mapping remains 4, but the total communication cost decreases to just 127 (Fig. 2.i).

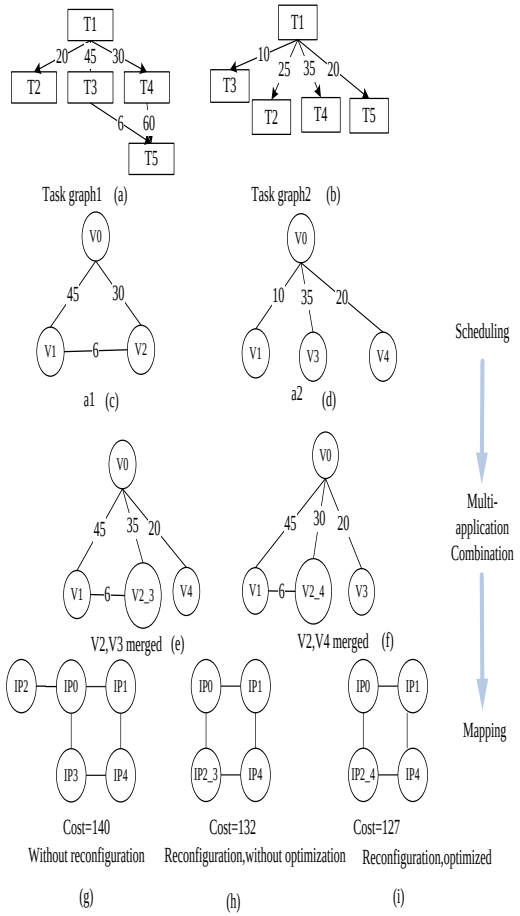

Fig. 2 An example showing Scheduling and Mapping with and without task merging through reconfiguration

The example illustrated in Fig. 2 has clearly indicated that communication cost can be effectively reduced without incurring additional hardware cost, if optimization on reconfiguration is performed along with scheduling and mapping.

This study thus attempts to develop a scheme that can effectively schedule and maps applications onto multiple IP cores, meanwhile taking into account of the reconfiguration cost. Due to its NP-completeness

in nature, we attempt to solve the problem following a design flow that includes three phases:

(1) During the scheduling phase (Phase 1), applications are scheduled onto the minimal number of virtual cores (as opposed to the physical IP cores) while meeting all the governing timing constraints.

(2) During the application merging phase (Phase 2), applications that can share the same virtual core but run at different time slots are identified, and these applications are thus considered to be merged to minimize the reconfiguration cost.

(3) During the final mapping phase (Phase 3), virtual cores are mapped to the physical cores in the way that the communication cost can be minimized. Note that the final NoC architecture is generated at this step.

4.1. Phase 1: Task scheduling

In this phase, the proposed task scheduling algorithm takes the number of virtual cores and the application task graphs as its input. Note that, instead of directly mapping tasks to physical cores connected by a NoC architecture, we actually schedule them onto virtual cores. The number of virtual cores can be equal to or greater than the number of physical cores. In our current implementation, the number of the virtual cores is set to be the same as that of the physical cores. The main idea of this scheduling step is to put the tasks into the same group if their run times do not overlap, and then assign one virtual core to each task group.

4.1.1. Scheduling Algorithm

This algorithm tries to find a schedule for each application represented by a task graph. The input to the algorithm is the task graph of an application, and the output is a core graph represented by virtual cores and their connections. For simplicity, run time of each task on a virtual core is set to be exactly one cycle. The objective of this scheduling algorithm is to minimize the number of virtual cores in the output graph under the timing constraint. There are three major steps in the algorithm.

Step 1, tasks are sorted by an ascending order of their start times.

Step 2, schedule the task in the task list that has the earliest start time (i.e., the first entry of the task list) onto an available virtual core. Once a task is scheduled, it will be deleted from the task list. Repeat this process until all the tasks have been scheduled.

Step 3, after all the tasks in the input task graphs have been scheduled onto the virtual cores, the connections among virtual cores have to be determined, following a policy given below:

--If two tasks in the task graph are scheduled onto the same virtual core, there is no need to add an edge between them.

--If two task in the task graph are determined to be scheduled onto two different cores, we need to (i) either find two virtual cores between which an edge shall be added, or (ii) specify the communication bandwidth between the two tasks, when an edge already exists between the two virtual cores.

Detailed scheduling algorithm is given below.

TaskScheduling {

Input:
T: Task Graph
P: list of available Virtual Core (VP) cores
Nv: the number of VP cores

Output:
The Core Graph of the application // see Def. 2 in Section II

Variable Declarations:
Here Q[v] records the time when virtual core, node v, becomes available;
D[v] records the set of tasks running at each IP core;
T_s^R records the start time of task R;
T_r^R records the run time needed to complete task R;
$T_s^R + T_r^R$ gives the scheduled time to complete task R.

Procedure body:

// Step 1
(1) Initialize array Q[v] of each VP core by setting array Q[v] to null, here v=1, 2,…Nv.
(2) Initialize the task set of each VP core by setting array D[v] to null, here v=1, 2,…Nv.;
(3) Sort the tasks in ascending order of start time and save the sorted tasks as task list T';

// Step 2
(4) If T' is not empty, assign the first element in T' to R, and then delete this element from T';

(5) Select node v from P such that Q[v] is minimized;

(6) Schedule R to v by assigning the start time and run time to R;

(7) Update Q[v] by having Q[v] <= $T_s^R + T_r^R$

(8) Add the first task in the list T' to D[v]

(9) Repeat lines between 4 and 8 until all the tasks in T' have been mapped onto VP cores.

// Step 3

(10) Add edges among Q[v];

(11) Return the generated Core Graph;

}

The complexity of this scheduling algorithm is bounded by the number of virtual cores. As each application is scheduled onto a virtual core through a two-loop iteration, the complexity of this algorithm is $O(|Nv|^2)$, where Nv is the number of virtual cores to be scheduled.

4.1.2. An Illustrative Example

We take the benchmark from TGFF [17] as an example to illustrate the proposed task scheduling algorithm. As can be seen from Fig. 3, there are 13 task nodes, of which maximum 5 tasks can be allowed to start at the same time. In this regard, at least 5 VP cores are needed to run all the tasks. The scheduling result after applying the proposed task scheduling algorithm is thus given as Fig. 4.

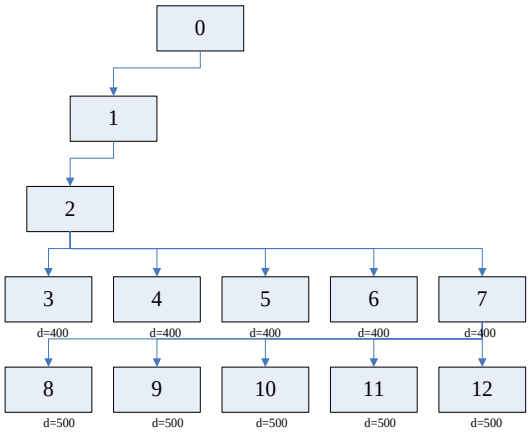

Fig. 3 A benchmark from TGFF[17]

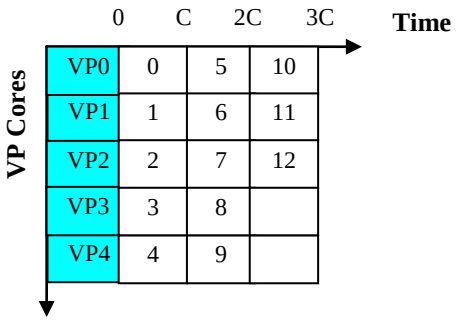

Fig. 4 Scheduling Result for the benchmark shown in Fig. 3

From Fig. 4, one can see that tasks 0, 5 and 10 have been scheduled to execute on virtual core 0 at the 0^{th}, the 1^{st}, and the 2^{nd} clock cycles, respectively. The other tasks have also been scheduled to execute on other virtual processors. The output core graph after task scheduling is shown in Fig. 5, where the weight of each edge corresponds to the communication cost between the two connecting VCs. For instance, communication cost between VP0 and VP1 is 491.

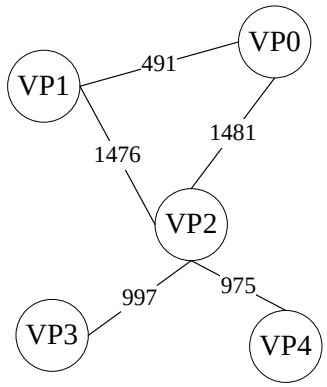

Fig. 5 Core Graph generated after task scheduling as shown in Fig.. 4

4.2. Phase 2: Merge of Multiple Applications and Minimization of Reconfiguration Cost

In Phase 2, the proposed algorithm takes the core graphs (each consists of virtual cores and weighted edges) obtained from phase 1 as its input, while the output is one merged core graph. The objective here is to minimize the number of virtual cores in the output core graph while satisfying the timing constraints.

4.2.1. Algorithm Description

This algorithm attempts to find two graphs, from the output core graphs obtained in Phase 1, that can be merged into one graph. This core graph merging process is repeated until no more graphs can be merged.

When an edge is identified to be merged with an existing edge, bandwidth between the two connecting virtual cores has to be updated to take the higher weight of the two edges. Then, two nodes can be merged assuming the longest communication bandwidth is maintained.

GraphMerging {

Input:

Two applications, Application1 and Application 2, represented by their respective core graphs cg1, and cg2

MT is set as time constraint condition

Output:

A core graph

Variable Declarations:

BW is the total communication bandwidth of a data flow graph.

OptimalCombine(cg1, cg2, MT){

1) Merge common Virtual Core (VP) cores of cg2 to cg1;
2) Sort VP cores in cg2 according to ascending order of their total communication bandwidths, and put them into a list, *L*;
3) If *L* is empty, go to Step 9;
4) Get the first element (VP core) of *L*, and is recorded as *n*;
5) Find core *m* from cg1 so that merging *m* with *n* will lead to the smallest BW;
6) If MT >0 then merge VP core *n* with *m* and then MT = MT-1;
7) Else Add *n* into dfg1 as a new VP core;
8) Delete *n* from *L* and go back to step3;
9) Update bandwidths of all the edges;

}

The complexity of the algorithm is determined by finding the virtual cores from the two input core graphs that shall be merged. For each virtual core of one graph (cg1), all the cores of the other graph (cg2) have to be traversed once (Step 5). The timing complexity is thus O ($N1 \times N2$), where *N*1and *N*2 are cg1 and cg2's numbers of the virtual cores, respectively.

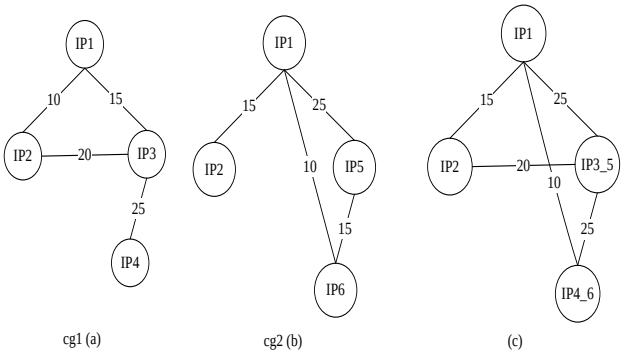

Fig.6 An Example showing merging of two core graphs (cg1 and cg2) to form a new core graph shown in (c) while minimizing communication bandwidth

4.2.2. An Illustrative Example

Suppose there are two core graphs, cg1 and cg2, derived from two applications, shown in Figs. 6.a and 6.b, respectively, and the timing constraint is set as 2. During the merging process, virtual cores IP1 and IP 2 in cg2 are first merged with the same virtual cores in cg1. Next, IP 5 and IP 6 in cg2 are put into the list L. After searching through cg1, IP3 in cg1 is merged with IP5 in cg2 since merging of these two will result in the lowest BW while still satisfying the timing constraints. Next, IP4 in cg1 and IP6 in cg2 are merged. Eventually, the merged core graph, with a communication bandwidth of 95, is shown in Fig. 6.c.

4.3. Phase 3: NoC mapping and optimization

The input of this phase is one core graph consisting of virtual cores and edges. The output of this phase is an mapped NoC architecture. The objective of this mapping step is to minimize the communcaiton cost under the timing and area constraints. There are three major steps in this algorithm. In the first step, an initial mapping is obtained, followed by a step where minimum path routing computation is performed. In the last step, the initial solution is iteratively improved by pair-wise swapping of nodes, and finally the NoC architecture is generated. That is, this algorithm attempts to map all the virtual cores to the physical cores of the NoC. As two or more virtual cores may be mapped to one core on NoC, communication cost of the NoC has to be considered in this phase.

4.3.1. Initialization

At the beginning, a mesh topology is first created with the minimum number of cores that shall be able to accommodate all the cores in the core graph. That is, for a core graph with N cores, a $\lceil N \rceil$ by $\lceil N \rceil$ mesh needs to be created. For instance, if there are 8 cores in the merged core graph, a mesh with 9 cores is created. The virtual core with the largest number of neighbors in the core graph is first mapped to an available core in the mesh with the largest number of neighbors. Next, of the core that have not to be mapped, the one which has the highest communication cost with the already mapped cores is selected for mapping. This procedure is repeated until all the cores in the core graph have been mapped onto the mesh architecture.

4.3.2. Routing Determination

The shortest routing is performed after the initial mapping. The total communication cost can be calculated using the shortest paths between any pairs of the source and the destination nodes. A quadrant graph is created between the source and the destination, as the shortest path between the source and the destination sits within the quadrant that they belong to. Then, Dijkstra's shortest path algorithm is applied to the quadrant graph and the minimum path is obtained.

4.3.3. Mapping Optimization and NoC Architecture Generation

In this phase, a heuristic simulate-annealing-based algorithm is used to generate the final mapped NoC topology with the minimum total communication cost. In essence, a pair of nodes are selected from the initial mesh (Section 4.3.1) and they get swapped, after which routing is performed to calculate the corresponding communication cost. If the communication cost of this newly mapped NoC topology is lower, it will be considered as a better solution and optimization will continue from this updated topology. Above procedure is repeated until no further optimization is possible, and the mapped NoC topology is finally generated. The complexity of this routine is relative to size of the mesh. As the number of nodes increases, there will be greater opportunities for node swapping.

V. Experimental Results

To evaluate the performance of the proposed algorithms as described in Section 4, a couple of experiments using an in-house developed platform have been performed. In specific, a 2D mesh-based NoC is designed with 16-bit wide channels. Routers in this NoC support wormhole packet switching and deterministic XY routing. Benchmarks include TGFF suites [17] and real-world applications.

In this first set of experiments, we apply the proposed algorithm to TGFF Benchmarks. Table 1 reports the scheduling results of 4 TGFF benchmarks after phase 1 (Section 4.1) is completed. In the second and third columns of the same table, the numbers of the nodes and the edges of the input task graphs are given,
respectively. For comparison, the fourth and the fifth columns, respectively, report the numbers of nodes and edges in the output core graph.

Table 1. Scheduling Results (Phase 1 described in Section 4.1)

Bench mark	No. Nodes At TG	No. of Edges at Task graph	No. of Nodes at Core Graph	No.of Edges at Core graph	Schedul-ing Time (Cycles)
tgff1	23	31	6	11	35
tgff2	18	23	5	9	30
tgff3	12	14	4	5	25
tgff4	15	22	4	6	30

The scheduling time is given in the sixth column, where each node is assumed to run at 5 clock cycles. It can be seen that after scheduling, the number of cores in the output core graph is much less than that of the tasks in the input task graph. Some tasks are scheduled to the same core to reduce the number of the nodes in the output core graph. The number of communication edges in the output core graph is also much lower than that of the input task graph for the same reason.

Table 2. Task Graph Merging Results

Bench mark	Nodes	Edges	Scheduling Time (Cycles) Before	Scheduling Time (Cycles) After
tgff1* tgff3	6	11	80	60
tgff2* tgff4	5	9	75	60
tgff2* tgff3 *tgff4	5	9	100	85
tgff1*tgff2* tgff3*tgff4	6	13	135	125

In the second column of Table 2, various combinations of TGFF benchmarks are shown. For instance, benchmark tgff1*tgff3 indicates that the core graphs of tgff1 and tgff3 are merged. In tgff1*tgff3, there are 6 nodes (the third column) and 11 edges (the forth column). When tgff1 and tgff3 are executed in series, a total of 80 cycles is needed (the fifth column)

as opposed to 60 cycles needed to schedule merged graph tgff1*tgff3 (the sixth column). In this case, the scheduling time of the merged graph is reduced by 15%. Here reconfiguration time between cores is set to be 2 cycles.

As certain cores can be reused through reconfiguration, the number of cores (nodes) in the merged graph is reduced dramatically, as shown in Fig. 7, which can be translated into significant area saving. Take the tgff1*tgff3 as an example: the number of cores is reduced.

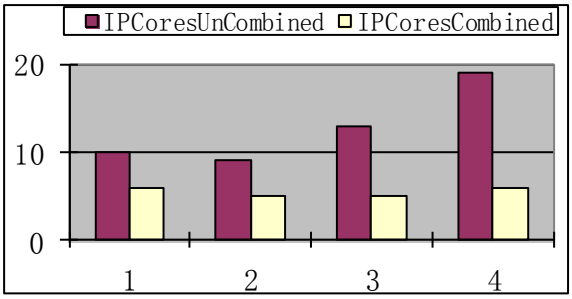

Fig. 7 the number of cores before the merging of the core graphs vs. the number of cores after the merging

from 10 (before merging) down to 6 (after merging). Finally, a merged graph is mapped to the actual mesh NoC, and the final mapping results are tabulated in Table 3. In our experiment, we define a hotspot on an NoC is a core that experiences 30% more traffic than an average core. In the third column, the number of hotspots on the NoC for each application after final mapping is given. For instance, both tgff1*tgff2 and tgff2*tgff4 have 2 hotspot while for the other two applications, each has 3 hotspots. It is shown that our algorithm applying on NoC with more hotspots can achieve more reductions on communication cost.

Table 3 Mapping Results of Various Applications onto NoCs

Benchmark	No. Cores	Hot Spot	Initial Comm. Cost without reconfiguration	Optimal Comm. Cost with reconfiguration
tgff1* tgff3	6	2	1785	1664
tgff2* tgff4	5	2	1998	1733
tgff2*tgff3 *tgff4	5	3	2014	1751
tgff1*tgff2 * tgff3*tgff4	6	3	2788	2200

In Table 3, the initial communication cost without reconfiguration is given in the fourth column, while the optimal communication cost with reconfiguration is reported in the fifth column.

For instance, an NoC with 6 cores (the second column) is generated for benchmark tgff1*tgff3, where 2 hotspots exist (the third column). The communication cost without reconfiguration is 1785 (the fourth column), while the communication cost is reduced to 1664 with reconfiguration (the fifth column). The most significant reduction on communication cost is achieved for benchmark tgff1*tgff2*tgff3*tgff4 (Table 3), where communication cost is reduced from 2788 cycles to 2200 cycles, a merely 21.2% reduction

B Evaluation of the proposed scheme using real applications running on a set-top box SoC

We have also evaluated the performance of the proposed algorithm by applying it to real-world applications. In particular, five applications run in a SoC for set-top box are adopted, as given in Fig.8. We present the experimental results for the applications running on 4 different configurations: (i) applications A1 and A2 running on P1, (ii) applications A2, A3 and A4 on P2, (iii) applications A1 ,A2 , A4 and A5 on P3, and (iv) applications A1, A2, A3, A4 and A5 on P4. After the merging algorithm is completed for each design (Phase 2 in Section 4.2), the results are given in the Fig. 9.

The numbers of cores before and after the merging process for all 4 designs are reported in Fig.10.a. For P1, 14 cores is actually needed if no core is merged (the second vertical bar in Fig. 10.a), and that number can be reduced to 7 (the first vertical bar in Fig. 10.a) if some cores can be shared. Across all four designs, on average, the number of cores needed is reduced by more than 50% with cores can be shared among applications through reconfiguration. Actually, one can see that the more cores can be shared, the more significant of area saving a design can achieve, as the case in P4.

The numbers of communication links before and after the merging process for all 4 designs are shown in Fig. 10.b.

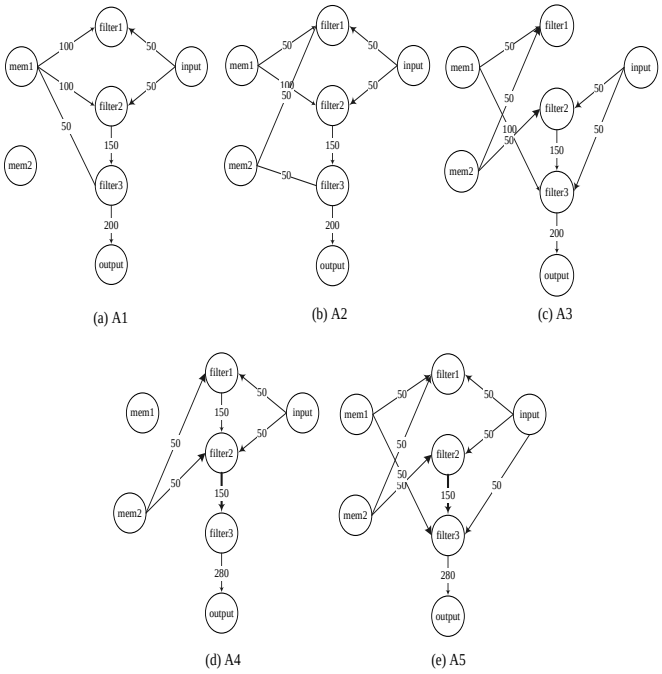

Fig. 8. Five applications running on a top-box SoC

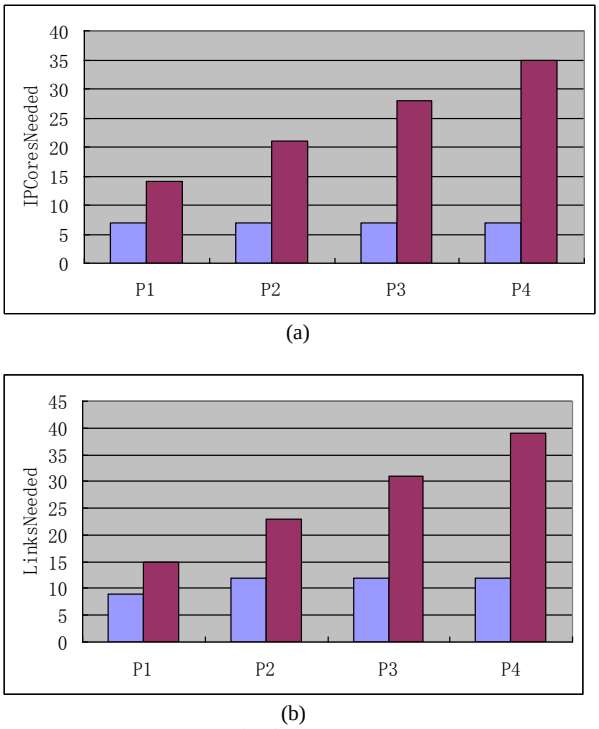

Fig10 Experimental results for four designs (a) Core reduction due to core sharing through reconfiguration (b) Communication link reduction due to core sharing through reconfiguration

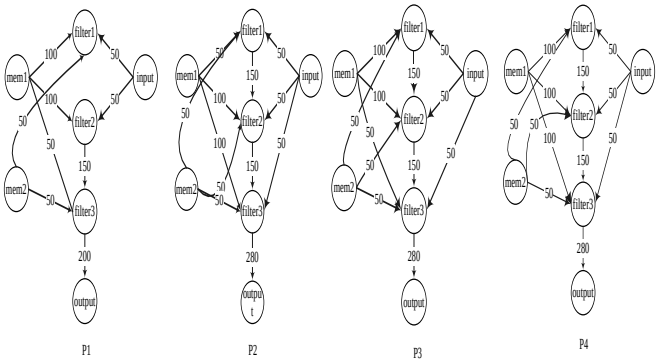

Fig. 9. The core graphs after merging for four designs.

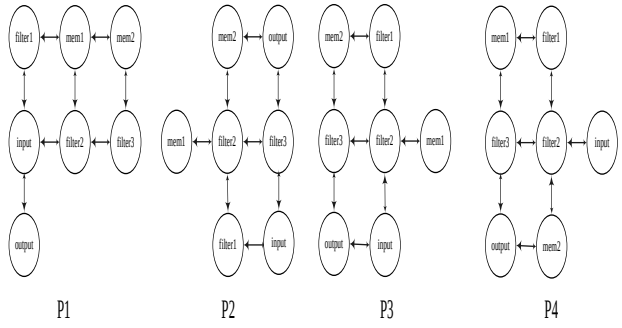

Fig.11. Optimal mesh topology generated

For P1, 15 links is actually needed if no core is merged (the second vertical bar in Fig. 10.b), and that number can be reduced to 9 (the first vertical bar in Fig. 10.b) if some cores are shared. Across all four designs, on average, the number of communication links needed is reduced by more than 50% when core sharing among applications is possible through reconfiguration. Actually, one can see that the more cores can be shared, the less communication links needed to connect all the communicating cores, as the case in P4.

Finally, the generated mesh architectures for each of the four designs are shown in Fig. 11.

VI. Conclusions

In this paper, a scheduling and mapping multiple applications on dynamically reconfigurable NoC was proposed to help minimize the communication cost, while satisfying the timing, area and other applicable design constraints. To save area, applications that can be mapped onto the same hardware resource but run at the different time instances through reconfiguration are identified, and the cost incurred in reconfiguration is actually considered along with application scheduling and mapping. The experiment results have shown that the proposed method has achieved 50% area reduction than a conventional scheme that does not consider reconfiguration cost.

Acknowledgement

The authors acknowledge the support from NSF of China (60706004 and 60876018).

References

[1] L. Möller, R. Soares, E. Carvalho, I. Grehs, N. Calazans, and F. Moraes, "Infrastructure for Dynamic Reconfigurable Systems: Choices and Trade-offs," *Proc. 19th annual symposium on Integrated circuits and systems design*. 2006:41-49

[2] L. Benini and G. De Micheli. *Networks on Chip: A New SoC Paradigm*. IEEE Computers. 2002:70-78

[3] S. Murali and G. De Micheli, "Bandwidth-constrained Mapping of Cores onto NoC Architectures," Proc. Design, Automation and Test in Europe Conference and Exhibition. 2004, 2: 896-901

[4] J. Hu and R. Marculescu, "Energy-Aware Communication and Task Scheduling for Network-on-Chip Architectures under Real-Time Constraints," *Design, Automation and Test in Europe Conference and Exhibition*. 2004:234-239

[5] D.Bertozzi, A. Jalabert, S. Murali, R.Tamhankar, S. Stergiou, L. Benini and G. De Micheli, "NoC Synthesis Flow for Customized Domain Specific Multiprocessor Systems-on-chip," *IEEE Trans. Parallel and Distributed Systems*, vol. 16, no. 2, pp. 113-159, Feb. 2005.

[6] K. Goossens, J. Dielissen, O.P. Gangwal, S. G. Pestana, A. Radulescu and E. Rijpkema, "A Design Flow for Application-Specific Networks on Chip with Guaranteed Performance to Accelerate SOC Design and Verification," *Proc. Design, Automation and Test in Europe Conference and Exhibition*. 2005:1182-1187

[7] T. Lei and S. Kumar, "A two-step Genetic Algorithm for Mapping Task Graphs to a Network on Chip Architecture," *Proc. Euromicro Symposium on Digital System Design*. 2003: 180-187

[8] K. Goossens, A. Radulescu and A. Hansson, "A Unified Approach to Constrained Mapping and Routing on Network-on-chip Architectures," *Proc. International Conference on Hardware-Software Codesign and System Synthesis*. 2005: 75-80

[9] J.Hu and R. Marculescu, "Exploiting the Routing Flexibility for Energy/ Performance Aware Mapping of Regular NoC Architectures," *Design, Automation and Test in Europe Conference and Exhibition*. 2003,1:1-6

[10] S. Murali, M. Coenen, A. Radulescu, K. Goossens and G. De Micheli, "A Methodology for Mapping Multiple Use-Cases onto Networks on Chips," *Proc. Design, Automation and Test in Europe Conference and Exhibition*. 2006, (1): 1-6.

[11] S. Murali, M. Coenen, A. Radulescu, K. Goossens and G. De Micheli, "Mapping and Configuration Methods for Multi-use-case Networks on Chips," *Proc. 11th Asia South Pacific Design Automation Conference*. 2006:1-6.

[12] A. Hansson, M. Coenen and K. Goossens, "Undisrupted Quality-of-Service during Reconfiguration of Multiple Applications in Networks on Chip," *Proc. Design, Automation and Test in Europe Conference and Exhibition*. 2007: 954-959.

[13] T. T. Ye, L. Benini and G.De Micheli, "Analysis of Power Consumption on Switch Fabrics in NetworkRouters," *Design Automation Conference*. 2002: 524-529

[14] R. Dick, D. Rhodes, and W. Wolf. "TGFF: Task Graphs For Free," *Hardware Software Codesign Conference*, pp. 97–101, 1998.

[15]I. Beretta, V. Rana, D. Atienza, and D. Sciuto, "A mapping flow for dynamically reconfigurable Multi-Core System-on-chip Design," *IEEE Trans. Computer Aided Design*, vol. 30, no.8, pp.1211-1224 , Aug. 2011.